HHS Public Access

Author manuscript

Cell. Author manuscript; available in PMC 2022 February 02.

Published in final edited form as:

Cell. 2019 May 30; 177(6): 1480–1494.e19. doi:10.1016/j.cell.2019.03.047.

Dual Sensing of Physiologic pH and Calcium by EFCAB9 Regulates Sperm Motility

Jae Yeon Hwang[1], **Nadja Mannowetz**[4], **Yongdeng Zhang**[2], **Robert A. Everley**[5], **Steven P. Gygi**[5], **Joerg Bewersdorf**[2], **Polina V. Lishko**[4], **Jean-Ju Chung**[1,3,6,*]

[1]Department of Cellular and Molecular Physiology, Yale School of Medicine, New Haven, CT 06510, USA

[2]Department of Cell Biology, Yale School of Medicine, New Haven, CT 06510, USA

[3]Department of Gynecology and Obstetrics, Yale School of Medicine, New Haven, CT 06510, USA

[4]Department of Molecular and Cell Biology, University of California, Berkeley, Berkeley, CA 94720, USA

[5]Department of Cell Biology, Harvard Medical School, Boston, MA 02115, USA

[6]Lead Contact

SUMMARY

Varying pH of luminal fluid along the female reproductive tract is a physiological cue that modulates sperm motility. CatSper is a sperm-specific, pH-sensitive calcium channel essential for hyperactivated motility and male fertility. Multi-subunit CatSper channel complexes organize linear Ca^{2+} signaling nanodomains along the sperm tail. Here, we identify EF-hand calcium-binding domain-containing protein 9 (EFCAB9) as a bifunctional, cytoplasmic machine modulating the channel activity and the domain organization of CatSper. Knockout mice studies demonstrate that EFCAB9, in complex with the CatSper subunit, CATSPERζ, is essential for pH-dependent and Ca^{2+}-sensitive activation of the CatSper channel. In the absence of EFCAB9, sperm motility and fertility is compromised, and the linear arrangement of the Ca^{2+} signaling domains is disrupted. EFCAB9 interacts directly with CATSPERζ in a Ca^{2+}-dependent manner

*Correspondence: jean-ju.chung@yale.edu.

AUTHOR CONTRIBUTIONS

J.-J.C. conceived and supervised the project. J.-J.C. and J.Y.H. designed, performed, and analyzed experiments. J.-J.C. created *Efcab9* null mice, did initial characterization, and contributed to all of the 4Pi-SMSN and SEM imaging. J.Y.H. performed comparative genomic screens and molecular and cell biology and protein chemistry experiments including expression construct generation, protein purification, immunocytochemistry, confocal and SIM imaging, and motility analysis. N.M. did electrophysiological recordings, and N.M., P.V.L., and J.-J.C. analyzed the electrophysiological data. Y.Z. performed 4Pi-SMSN imaging, image analysis, and rendering. J.-J.C. and R.A.E. performed proteomic experiments, and J.-J.C., J.Y.H., and R.A.E. analyzed the proteomic data. S.P.G., J.B., and P.V.L. provided crucial reagents and equipment. J.Y.H. and J.-J.C. assembled figures and wrote the manuscript with the input from the co-authors.

DECLARATION OF INTERESTS

The authors declare no competing interests. J.B. is a consultant for Bruker Corp. and holds several patents on super-resolution microscopy techniques.

SUPPLEMENTAL INFORMATION

Supplemental Information can be found online at https://doi.org/10.1016/j.cell.2019.03.047.

and dissociates at elevated pH. These observations suggest that EFCAB9 is a long-sought, intracellular, pH-dependent Ca^{2+} sensor that triggers changes in sperm motility.

In Brief

A pH-dependent calcium sensor enables modulation of sperm motility in response to changing conditions along the female reproductive tract.

Graphical Abstract

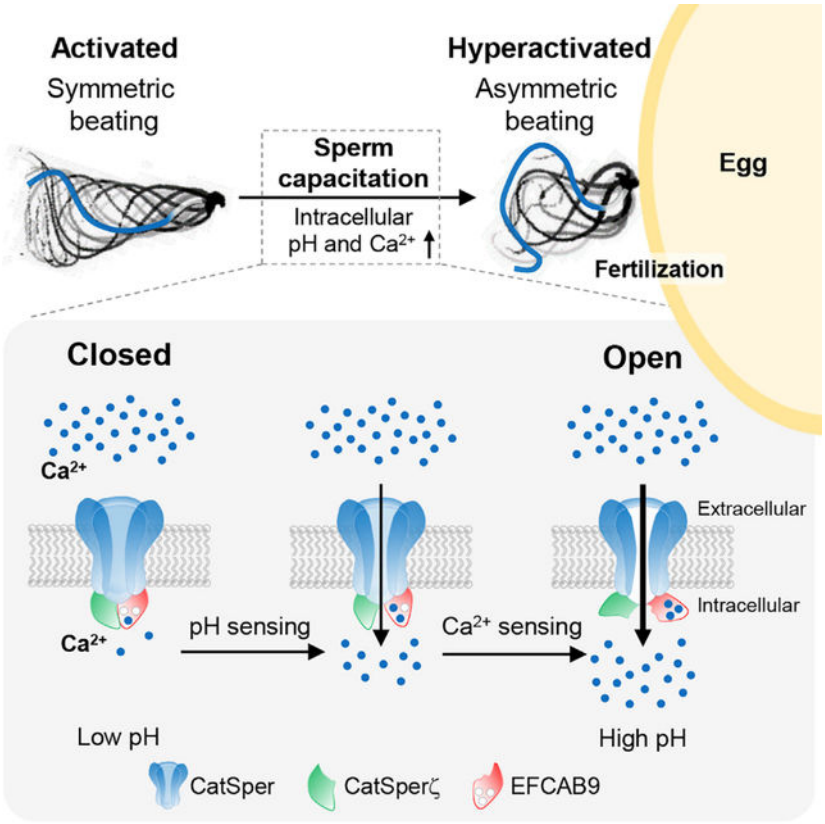

INTRODUCTION

Changes in sperm motility patterns (Yanagimachi, 1970, 2017), observed in the steering chemotactic movement of marine invertebrates (Böhmer et al., 2005; Wood et al., 2005) and triggering hyperactivated motility in mammals (Ho and Suarez, 2001; Suarez et al., 1993), require Ca^{2+} influx across the flagellar membrane. The molecular commonalities for this Ca^{2+} entry into sperm cells are the flagella-specific and Ca^{2+}-selective channel, CatSper (Carlson et al., 2003; Qi et al., 2007; Quill et al., 2003; Ren et al., 2001; Seifert et al., 2015) and its activation by intracellular alkalinization (Kirichok et al., 2006; Lishko et al., 2010, 2011; Miller et al., 2016; Seifert et al., 2015; Strünker et al., 2011). This implies that an evolutionarily conserved pH sensing mechanism regulates the CatSper channel. By contrast, whether such modulation requires cytosolic Ca^{2+} has not been directly demonstrated,

although it has been postulated based on studies of non-spermatozoan, voltage-gated Ca_V channels (Catterall, 2011).

The CatSper channel is the most complex of all known ion channels, encoded by at least nine genes in mammals. It consists of pore-forming α subunits (CatSper1–4) (Qi et al., 2007; Quill et al., 2003; Ren et al., 2001) and five accessory subunits (transmembrane CatSperβ, CatSperγ, CatSperδ, CatSperε, and cytosolic CatSperζ) (Chung et al., 2011, 2017; Liu et al., 2007; Wang et al., 2009). Male mice lacking CatSper genes (Chung et al., 2011, 2017; Quill et al., 2003; Ren et al., 2001), as well as humans with loss of function mutations (Avenarius et al., 2009; Brown et al., 2018; Hildebrand et al., 2010; Luo et al., 2019; Smith et al., 2013), in transmembrane (TM) subunits are completely infertile due to lack of sperm hyperactivation. Greater understanding of regulatory mechanisms has been hampered by the inability to heterologously reconstitute the complex channel and the inseparability of sperm phenotypes resulting from loss of each TM subunit in mice (Carlson et al., 2005; Chung et al., 2011, 2017; Qi et al., 2007). Amino acid properties and sequence homology of subunits have been used to speculate on the molecular mechanism of this pH-dependent activation of the channel. Moreover, to date, none of the known CatSper subunits contained calcium/CaM binding motifs, suggesting that additional proteins assist complex assembly and trafficking, and/or detect changes in intracellular pH and Ca^{2+} for the CatSper channel.

The recent identification of CatSperζ (Chung et al., 2017) as a unique cytoplasmic component of the mammalian CatSper complex has been illuminating. CatSper organizes Ca^{2+} signaling nanodomains, uniquely aligned along the sperm tail as “racing stripes” to form a network of intracellular signaling molecules (Chung et al., 2014). Contrary to other CatSper knockout models, CatSperζ deficiency disrupts the CatSper domains, but the channel is functional and only results in *CatSperz* null male subfertility (Chung et al., 2014, 2017). These studies indicate that CatSperζ functions in the compartmentalization of Ca^{2+} signaling in mammalian sperm and may modulate the Ca^{2+} influx mechanism of the CatSper channel.

Here, we use comparative proteomic and genomic screens and identify EFCAB9, a sperm-specific EF-hand protein, as a new CatSper auxiliary subunit that modulates channel activity and domain organization. We develop an *in vivo* mouse model to examine EFCAB9 function at the molecular, cellular, biochemical, electrophysiological, and super-resolution imaging levels. EFCAB9 is a pH-dependent Ca^{2+} sensor for the CatSper channel and a direct binding partner of CatSperζ. EFCAB9-CatSperζ protein pairs interact with the channel pore as a gatekeeper before capacitation but activate the channel in response to capacitation-associated intracellular pH and Ca^{2+} changes. EFCAB9 interaction with CatSperζ requires Ca^{2+} binding to EF-hands, which respond to pH changes in a physiological range. Loss of EFCAB9-CatSperζ largely eliminates the pH-dependent activation of CatSper, impairs CatSper regulation by intracellular Ca^{2+}, and alters newly resolved substructures of CatSper Ca^{2+} signaling domains. In contrast to the recent addition of CatSperζ to mammals, EFCAB9 is evolutionarily conserved from flagellated single-cell eukaryotes as other transmembrane CatSper subunits. These findings provide insight into evolutionarily

conserved gating mechanisms for CatSper channels and reveal an adaptation for Ca^{2+} signaling in flagella.

RESULTS

Comparative Proteomic and Genomic Screens Identify Components of CatSper Calcium Channel Complex in Sperm

Sperm hyperactivated motility requires pH-dependent activation of the CatSper flagellar Ca^{2+} channel. The CatSper channel forms a multi-protein complex composed of at least nine subunits (CatSper1–CatSper4, CatSperβ, CatSperγ, CatSperδ, CatSperε, and CatSperζ) (Chung et al., 2017). Here, we examine a new member of the complex and determine its functional significance.

Our previous studies showed that other CatSper subunits were not detected in the epididymal sperm cells from *CatSper1* and *d* null mouse males despite their protein expression in testis (Chung et al., 2011, 2017). To identify new CatSper components based on this interdependence, we performed a quantitative whole sperm proteomic screen to compare *CatSper1* null with wild type (WT) sperm (Figure 1A), concomitant with our previous phosphotyrosine proteome analysis (Chung et al., 2014). Using tandem mass tag (TMT) labeling and mass spectrometry analysis, we quantified 3,227 proteins from *CatSper1* null and WT spermatozoa (Figure 1A), comparable to the size of other mouse sperm proteome (Castaneda et al., 2017). In the experiment run in triplicate, only 19 proteins (14 downregulated and 5 upregulated significantly at $p < 0.05$) were differentially expressed in *CatSper1* null sperm by more than 2-fold (Figure 1A; Table S1). This overall lack of differential protein expression between WT and *CatSper1* null spermatozoa is particularly remarkable because our screen still identified all nine known transmembrane and cytosolic components of the CatSper channel complex in a precise, quantitative, and reproducible manner (Figure 1A). This result validates the accuracy of the data and strongly suggests that proteins missing from mature *CatSper1* null spermatozoa normally form a stable complex with the CatSper channel. Thus, five additional downregulated proteins are strong candidates for CatSper components that are unincorporated into the flagellar membrane or degraded in the absence of the CatSper channel.

To further validate the five candidates, we defined two additional criteria, based on the characteristics common to the known CatSper components: (1) be testis-specific with postmeiotic expression, and (2) share evolutionarily conservation patterns of lineage-specific gain and loss of *CatSper* genes. *Efcab9* meets both criteria (Figures S1A and S1B).

EFCAB9 Is an Intraflagellar Protein with Conserved EF-Hand Ca^{2+} Binding Domains

Amino acid sequence alignment of EFCAB9 to calmodulin (CaM) predicts that EFCAB9 has three conserved EF-hand Ca^{2+} binding domains (Figure 1B). The conserved helix-loop-helix motifs (EF1–EF3) contain candidate EF-hand Ca^{2+} binding sites (Figures S2A and S2B). EF-hand Ca^{2+} binding sites are the side chains of aspartic and glutamic acids located in each loop (Figures 1B and S2A–S2C). Interestingly, sequence comparison of the EF loops of EFCAB9 orthologs revealed species-specific variations in EF1 and EF2 from the

canonical EF loop containing an acidic residue at position 12 (Figure S2C). EFCAB9 was tightly clustered with all reported CatSper subunits in our proteomic analyses as one of the most reduced proteins in *CatSper1* null spermatozoa (Figure 1A; Table S1). We confirmed that *Efcab9* is expressed only in the testis, which contrasts with the genes encoding other EF-hand containing proteins including CaM and EFCAB1 (Figure S1C; Table S1). *Efcab9* transcripts are detected after meiosis, similar to the CatSper genes encoding the pore-forming α-subunits and unlike the other auxiliary subunits (Figure S1D) (Chung et al., 2011, 2017). We compared the protein expression and subcellular localization in WT sperm cells with those in *CatSper1* and *CatSperd* null spermatozoa (Figures 1C–1E) by a EFCAB9-specific antibody (Figures S2D, S2E, and S3C). EFCAB9 is localized to the principal piece of the WT mouse and human sperm tail (Figures 1E and 1F), as are other CatSper subunits, but is not detected in mouse sperm lacking the CatSper channel (Figure 1D). 3D structured illumination microscopy (SIM) imaging revealed localization in the characteristic four linear domains of sperm flagella (Figure 1G). From these results, we hypothesized that EFCAB9 is a functionally relevant CatSper component. The EF-hand is one of the major Ca^{2+}-binding regions found on many of the Ca^{2+} sensors including CaM (Clapham, 2007), and EFCAB9 is the first CatSper component with a known, conserved domain. This raises the question of whether EFCAB9 underlies Ca^{2+} sensing of the CatSper channel to regulate sperm hyperactivated motility.

EFCAB9-Deficient Mice Have Reduced Male Fertility and Phenotypes Resembling Loss of CatSperζ Function

To examine the potential role of EFCAB9 in the CatSper-mediated Ca^{2+} signaling pathway, we created *Efcab9* knockout mice by CRISPR/Cas9 genome editing (Figures 2 and S3). We obtained two mutant alleles with either a 5 bp (*Efcab9–5del*) or a 28 bp (*Efcab9–28del*) deletion. These two mutant lines showed identical phenotypes in our initial characterization of bi-allelic homozygous (null) mice, ruling out the possibility that off-target effects account for the phenotypes we observed. We used the *Efcab9–28del* mutant line as the *Efcab9* null mouse in this study unless indicated otherwise. Mutant mice lacking EFCAB9 (Figures 2H and S3C) showed no gross abnormality in appearance, behavior, or survival. *Efcab9* null females had normal mating behavior and gave birth to litters when mated with WT or mono-allelic heterozygous (het) males. However, fertility was severely impaired in *Efcab9* null males (Figures 2A, 2B, and S4A), despite normal sperm morphology and epididymal sperm count (Figures 2H and S4B). Pregnancy rate of null males was 36% (Figure 2A), compared to 100% for het, although the null males did not show any difference in mounting behaviors or plug formation. The fertilization rate of *Efcab9* null sperm was also significantly reduced *in vitro* (Figure 2B). Finally, litters sired by *Efcab9* null males were smaller than litters sired by het males (Figure S4A), suggesting null males are subfertile.

We further examined flagellar beating pattern (Figures 2C and 2D; Video S1). Incubating under capacitating conditions increased the amplitude of lateral movement, measured as the maximum angle within the midpiece (α-angle) (Qi et al., 2007), slowing the beat frequency of *Efcab9* het sperm (Figures 2E and 2F; Video S1). In contrast, the beat frequency of *Efcab9* null sperm, which is faster than het spermatozoa, did not change by capacitation. Importantly, Efcab9 null spermatozoa displayed stiff flagella with a fixed curvature from

the midpiece to the proximal region of the principal piece (Figures 2D and 2G; Video S1). Because the head of mouse sperm is curved like a sickle with an apical hook, the direction of flagellar bending can be defined as pro-hook or anti-hook (Figure 2C) (Ishijima et al., 2002). The majority of the *Efcab9* null sperm retained an anti-hook bend (Figures 2D and 2G), suggesting that EFCAB9 functions in the CatSper-mediated Ca^{2+} signaling pathway that normally results in the pro-hook bend (Chang and Suarez, 2011). Genetic disruption (Chung et al., 2014, 2017) or pharmacological inhibition (Navarrete et al., 2015) of CatSper potentiates protein tyrosine phosphorylation (P-Tyr), a biochemical hallmark of sperm capacitation (Visconti et al., 1995). Therefore, elevation of the capacitation-associated P-Tyr in *Efcab9* null sperm (Figure S4C) indicates the CatSper-mediated Ca^{2+} current was aberrant, further supporting EFCAB9 regulation of CatSper. As reported in *CatSper1* null sperm, other proteins targeted to the signaling nanodomains might have been delocalized in *Efcab9* null spermatozoa. We investigated whether EFCAB9 deficiency dysregulates the localization and/or expression of the CatSper complex in sperm cells. SIM images of CatSper1 revealed that the structural continuity of the linear arrangement is interrupted in the absence of EFCAB9 while the CatSper complex remains targeted to the flagellum (Figure 2H). In *Efcab9* null sperm, we found all CatSper TM subunits express at 20%–30% of their normal range (Figures 3A and 3B), identical to the *CatSperz* null phenotypes (Chung et al., 2017). A reduced maximal CatSper-conducted whole cell current was recorded in *CatSperz* null spermatozoa (Chung et al., 2017). Likewise, we predict that a functional channel would form in the absence of EFCAB9. It would be intriguing to test whether this change is simply due to the reduced levels and the altered arrangement of the channels or involves any different biophysical properties of the channels. Thus, we set out to determine if EFCAB9 and CatSperζ form a functionally relevant complex, followed by electrophysiological analyses.

EFCAB9 Forms a Binary Complex by Interacting Directly with CatSperζ

Comparing *Efcab9* null mice with the *CatSper1*, *d*, and *z* knockout lines, EFCAB9 and CatSperζ protein expression is strictly interdependent (Figure 3). In contrast, neither is required to express CatSper channel (Figures 2H, 3A, and 3B), but each modulates the protein expression levels and organization of CatSper signaling domains (Figure 2H) (Chung et al., 2017). To further assess their functional interaction, we generated double knockout males (*Efcab9*$^{-/-}$; *CatSperz*$^{-/-}$). We did not observe any difference in defects of the males (Figures S4D–S4F) compared with those of single *Efcab9* or *CatSperz* null males (Figure 2) (Chung et al., 2017). These mice were severely subfertile with ~33% pregnancy rates in mating studies (Figure S4E). Sperm from double knockout males failed to develop hyperactivated motility and displayed flagellar waveforms similar to those observed in single *Efcab9* or *CatSperz* null sperm (Figures 2D–2G and S4F) (Chung et al., 2017). Double knockout sperm also express CatSper proteins comparable to those of *Efcab9* null sperm cells (Figure S4G), showing loss of continuity in the linear CatSper domains (Figure S4H). These results demonstrate no additive or synergistic defects in the loss of both proteins, strengthening the conclusion that EFCAB9 and CatSperζ are dispensable for CatSper channel expression.

To determine whether EFCAB9 binds CatSperζ, we carried out co-immunoprecipitation (coIP) and pull-down analysis. Both EFCAB9 and CatSperζ are complexed with the other protein in 293T cells transiently expressing EFCAB9 and CatSperζ (Figure 4A). We purified recombinant mouse EFCAB9 and CatSperζ proteins fused to either glutathione S-transferase (GST) or 6xHis-GB1 from *E. coli* and used for *in vitro* binding assays. Although non-specific interaction of GST-EFCAB9 with Ni^{2+} resin was observed, GST or His-tag pull-down analysis revealed that EFCAB9 and CatSperζ are direct binding partners (Figure 4B).

The EF-Hands of EFCAB9 Mediate Ca^{2+}-Sensitive Interaction with CATSPERζ

Next, we examined whether EFCAB9-CatSperζ interaction is Ca^{2+}-sensitive. Because GST-tag pull-down offers specific binding, all the following pull-down experiments were performed using the GST-tagged EFCAB9. Pull-down analysis revealed a strong interaction between EFCAB9 and CatSperζ under conditions without added Ca^{2+} (nominal free Ca^{2+}, typically ~10 μM free Ca^{2+}) or with 2 mM Ca^{2+} at pH 7.5 (Figures 4C, middle, and 4D). In contrast, when Ca^{2+} is chelated, EFCAB9 and CatSperζ dissociate, and binding is significantly reduced. These results indicate that Ca^{2+} is required for a stable EFCAB9-CatSperζ interaction, and Ca^{2+} likely binds to the EF-hands of EFCAB9.

We tested whether the Ca^{2+}-sensitive interaction is due to the Ca^{2+} binding ability of EFCAB9, by generating a charge-neutralizing EFCAB9 mutant ($EFCAB9^{Mut}$, Figures 1B and 4C). We substituted the conserved aspartate and glutamate located at the ends of the EF1 and EF3 loops to asparagine and glutamine (D72N/E160Q). $EFCAB9^{Mut}$ has significantly reduced binding to CatSperζ (Figures 4C, left, and 4D), suggesting the mutations attenuate Ca^{2+} binding of EFCAB9. Diminished $EFCAB9^{WT}$ binding to CatSperζ by chelating free Ca^{2+} (Figure 4C, middle) suggests that EFCAB9 interacts with CatSperζ in its Ca^{2+}-bound form. Ca^{2+} binding to $EFCAB9^{Mut}$ is partly rescued by adding 2 mM Ca^{2+} (Figures 4C, right, and 4D). These results confirm that the EF-hands of EFCAB9 mediate Ca^{2+}-sensitive interaction, and EFCAB9, in complex with CatSperζ, can function as a Ca^{2+} sensor for the CatSper channel. Thus, EFCAB9-CatSperζ appears to be important for both modulating channel activity and organizing the CatSper domains.

EFCAB9-CatSperζ Is Required to Link Two Rows with in a Single CatSper Domain

The CatSper channel complex forms unique longitudinal Ca^{2+} signaling nanodomains with other Ca^{2+} signaling molecules as four linear quadrants in the sperm flagellar membrane (Chung et al., 2014, 2017). The intact, high level of 3D organization of CatSper nanodomains is required to time and/or maintain hyperactivated motility (Chung et al., 2014, 2017). These structures are specific adaptations of Ca^{2+} compartments, such as ones found in neuronal synapses and cilia (Clapham, 2007), to efficiently coordinate Ca^{2+} signaling along the extremely long, narrow tail during hyperactivated motility. Recently, Miller et al. (2018) reported that H^+ channels in human sperm show bilateral organization, distinct from the quadrilateral arrangement of the mouse and human CatSper (Chung et al., 2017). These results suggest that different nanoscale organization of ion channels and its effector proteins could spatio-functionally regulate flagellar motility patterns. Our previous Immunogold electron microscope (EM) images of CatSper1 (Chung et al., 2014) suggested a two-row

structure within each longitudinal CatSper compartment. In the absence of EFCAB9 (Figure 2H) and/or CatSperζ (Figure S4H), the four lines are interrupted at repeated intervals (Chung et al., 2017). However, a typical transmission EM shows only a subsection of a flagellum and standard STORM imaging with 20- to 50-nm 3D resolution did not clearly resolve the paired structure. Recently developed, 4Pi single-molecule switching nanoscopy (4Pi-SMSN) enables improved resolution of 10- to 20-nm in three dimensions (Huang et al., 2016). We employed the 4Pi-SMSN to further assess the potential substructure and the effect of EFCAB9-CatSperζ on the spatial organization within the quadrant.

We first imaged CatSper domains in WT sperm by immunolabeling with a verified CatSper1 antibody (Chung et al., 2014; Ren et al., 2001). Consistent with our previous findings, the CatSper domains are distinct linear quadrants along the principal piece of the flagella (Figures 5A and 5C; Video S2). Closer inspection revealed that each quadrant is further resolved to a two-row structure, as clearly demonstrated in the cross-sections of the flagellum (Figure 5A; Video S2). The 2D angular distributions of the surface localizations (Figure 5B) also hint at two tight lines within a domain (Figure 5C). Interestingly, the linear CatSper domains are not only disrupted at periodic intervals, but the two-row structure within a domain appears to be irregular and organized in a single row in the absence of EFCAB9-CatSperζ (Figures 5A and 5C; Video S3). These results illustrate that CatSper double-row organization requires EFCAB9-CatSperζ.

Micron-scale membrane subdomains have been demonstrated in terms of lipid segregation in the sperm head (Selvaraj et al., 2006). In sperm tails, a distinct membrane subdomain known as the flagellar zipper was reported (Friend and Fawcett, 1974; Selvaraj et al., 2007), but the function and molecular basis of this structure remains a mystery. We asked whether sperm tail membrane subdomains, representing the macromolecular CatSper complex, can be visible by scanning EM(SEM). We identified a doublet of raised linear surface domains in WT sperm, running each side of the longitudinal columnar surface structure down the principal piece (Figure 5D, left). One doublet is made of two ~20 nm thick membranous stripes. The absence of these raised stripes in the SEM images of *CatSper1* null sperm (Figure 5D, right) indicates that these linear surface domains may be a protein-based membrane compartmentalization composed of the CatSper channel complex. The shorter fragmented singlet observed in *Efcab9* null sperm flagella (Figure 5D, middle) supports the conclusion that EFCAB9-CatSperζ has a structural function in organizing doublet CatSper domains seen in the sperm surface nanoarchitecture.

EFCAB9-CatSperζ Complex Confers pH-Dependent Activation and Ca^{2+} Sensitivity to CatSper Channel

A rise in intracellular pH potentiates $I_{CatSper}$ (Kirichok et al., 2006), which regulates sperm motility. In light of the reduced average whole cell $I_{CatSper}$ amplitude in *CatSperz* null sperm (Chung et al., 2017) together with the new findings of the Ca^{2+}-dependent interaction between EFCAB9-CatSperζ protein pairs (Figures 3, 4, and S4), we next examined whether the loss of EFCAB9 and CatSperζ altogether affects the pH-dependent activation and cytosolic Ca^{2+} sensitivity of the CatSper current upon voltage changes. A reduced current can reflect changes in the number, open probability (P_o), or elementary conductance of the

channels. Given peculiarities of reduced protein expression of other CatSper subunits in *CatSperz* null, *Efcab9* null, and double knockout sperm, we characterized $I_{CatSper}$ densities (pA/pF) (Figures 6A–6F and S5).

Interestingly, with genetic disruption of *CatSperz*, which results in spermatozoa lacking both EFCAB9 and CatSperζ, current densities recorded from *CatSperz* null sperm cells were similar to WT (pH 6.0) (Figures S5A–S5E). This suggests that the CatSper channels not associated with EFCAB9-CatSperζ are likely to have higher open probability and/or elementary conductance than those of WT, despite the reduced levels and the altered arrangement of channels. At higher negative and positive voltages, CatSper currents are even slightly larger in *CatSperz* null sperm cells, but because these are outside the physiological range, are of uncertain significance. In agreement with previous findings (Kirichok et al., 2006), $I_{CatSper}$ densities increase dramatically in WT spermatozoa when 10 mM NH_4Cl is added (Figures S5A–S5E). In contrast, *CatSperz* null sperm showed only a modest response (Figures S5A–S5E), suggesting compromised channel activation by intracellular alkalinization. These results provide evidence that EFCAB9-CatSperζ regulates pH-dependent CatSper activation.

Low free Ca^{2+} (<10 nM, buffered by 2 mM EGTA) largely eliminated the interaction between EFCAB9 and CatSperζ *in vitro* (Figures 4C and 4D). To directly test the Ca^{2+} sensitivity of the pH-dependent CatSper activation, we recorded the currents with buffered [free-Ca^{2+}] at a fixed intracellular pH in pipette (Figures 6A–6F and S5F). Because CatSper normally would not conduct Ca^{2+} outward under the physiological extracellular Ca^{2+} concentrations, the inward CatSper currents were mainly examined. At acidic intracellular pH (pH_i = 6.0), CatSper channel did not conduct inwardly in both WT and *Efcab9* null sperm during voltage step regardless of intracellular Ca^{2+} concentrations, particularly in the physiological range. This result suggests that the apparent Ca^{2+} sensitivity of the CatSper channel is low at acidic pH, preventing full-channel activation, perhaps due to the increasing interaction between EFCAB9 and CatSperζ. However, alkaline intracellular pH (pH_i = 7.4) dramatically potentiated CatSper channel activation in WT sperm (12- to 20-fold) in a concentration-dependent manner but to a much lower degree in *Efcab9* null sperm (~5-fold) in the presence of intracellular free Ca^{2+} (Figures 6A–6F and S5F). 10 μM corresponds to Ca^{2+} levels in the vicinity of calcium channels upon Ca^{2+} entry (Naraghi and Neher, 1997). Thus, pH presumably tunes the Ca^{2+} sensitivity of EFCAB9, triggering a conformational change, which alters the affinity of EFCAB9 for CatSperζ within the protein pairs.

To better understand the pH-dependent Ca^{2+} gating mechanisms of CatSper by EFCAB9-CatSperζ, we performed GST pull-down of EFCAB9/CatSperζ interactions at varying pH in nominal free Ca^{2+} solution (Figures 6G and 6H). We found that the amount of CatSperζ bound to $EFCAB9^{WT}$ gradually decreases when pH is raised (Figure 6G, left, and 6H). The interaction is further diminished when pull-down was performed with $EFCAB9^{Mut}$ (Figure 6G, right, and 6H). These data support that EFCAB9 is a pH-dependent Ca^{2+} sensor to activate CatSper channel, indicating that evolution developed ways to limit CatSper-mediated Ca^{2+} entry before capacitation-associated intracellular alkalinization in mammals.

EFCAB9-CatSperζ Interacts with Cytoplasmic Mouth of CatSper Channel Pore

The native CatSper channel is comprised of the pore (heterotetrameric CatSper1, 2, 3, 4) (Qi et al., 2007) complexed with the auxiliary subunits β (Chung et al., 2011; Liu et al., 2007), γ (Chung et al., 2011; Wang et al., 2009), δ (Chung et al., 2011), ε, and ζ (Chung et al., 2017). The order of assembly and the stoichiometry of each auxiliary subunit with the pore remains unknown. The native CatSper complex from mature sperm is not solubilized (Figure S2F), presumably due to the complex composition and organization into highly ordered arrays (Figures 3 and 5). Therefore, we performed coIP in a heterologous system and pull-down assays using purified recombinant proteins (Figures 7A and S6A–S6C) to examine the molecular interaction between cytosolic EFCAB9-CatSperζ and individual CatSper TM subunits. HA-tagged EFCAB9 and V5-tagged CatSperζ were transiently expressed in 293T cells with one of the CatSper subunits. The EFCAB9-CatSperζ complex interacts with each of CatSper1–CatSper4 (Figures 7A, S6A, and S6B) but has little to no interaction with the auxiliary TM subunits (β, γ, δ, and ε) (Figure S6C). These data are consistent with the hypothesis that EFCAB9-CatSperζ interacts with the channel pore (Figures 7B).

The remarkably histidine-rich N terminus of mammalian CatSper1 was suggested as a candidate for the pH-sensor of the CatSper channel (Kirichok et al., 2006; Ren et al., 2001). Our electrophysiology results strongly suggest that the EFCAB9-CatSperζ complex can account for the pH-dependence of channel activation to a large extent, but the absence of the protein pairs did not completely eliminate the pH sensing of the channel (Figures 6 and S5). Interestingly, pairwise-distance analysis of amino acid sequences showed that the CatSper1 N-terminal domain and CatSperζ are highly divergent among mammals in contrast to EFCAB9 and other cytoplasmic domains of CatSper α subunits (Figure S6D), suggesting specific co-evolution. Unlike other CatSper subunits and EFCAB9, CatSperζ is conserved specifically among mammals (Figure S1B). Thus, we hypothesized that CatSperζ fine tunes Ca^{2+} sensing via EFCAB9 by interacting with the CatSper1 N-terminal histidine-rich domain in a pH-dependent manner. We tested this idea by performing pull-down analysis between amino (N1–150) or carboxyl (C574–686) terminus of CatSper1 and the CatSperζ or EFCAB9-CatSperζ complex (Figures S6E–S6G). We found no evidence of direct interaction between either the C- or N-terminal domain of CatSper1 and EFCAB9-CatSperζ or CatSperζ (Figures S6F and S6G). This does not, however, rule out the possibility that the CatSper1 N terminus has a separate pH-dependent effect on gating or that it binds Zn^{2+} or other modulators.

EFCAB9-CatSperζ Is Required for Efficient Ca^{2+} Handling for Sperm Motility Regulation

Thus far, our results suggest that EFCAB9 rapidly senses changes in pH and Ca^{2+} and alters its association with CatSperζ and likely with the channel pore, resulting in more calcium entry. During sperm tail formation, EFCAB9-CatSperζ coordinates the channel complex trafficking into the spatially organized nanodomains (Figure 5) (Chung et al., 2017). A transient Ca^{2+} pulse by a Ca^{2+} ionophore, A23187, lessens the rigidity of the proximal tail of *CatSperz* null spermatozoa, but fails to fully rescue motility defects (Chung et al., 2017). In the absence of EFCAB9-CatSperζ, the channel is less sensitive to intracellular Ca^{2+} changes (Figures 6A–6F). These results suggest that the initial priming by Ca^{2+} influx can bypass the CatSper spatial organization to develop some hyperactivated motility, but

motility regulation for a longer period requires the maintenance of Ca^{2+} homeostasis. We thus examined how WT, *Efcab9* null, and *CatSper1* null sperm handle intracellular Ca^{2+} changes to regulate sperm motility and flagellar shape (Figures 7C and S7).

We observed that the initial total motility of *Efcab9* null sperm, measured by computer-assisted semen analysis (CASA), is lower by 10% than those of WT and *CatSper1* null sperm before capacitation (Figure 7C, M2). When intracellular Ca^{2+} was reduced by 5 μM BAPTA-AM under non-capacitating conditions, the motility of *Efcab9* null sperm was reduced faster than WT and *CatSper1* null sperm (Figures 7C and S7, BAPTA-AM versus vehicle in M2; Videos S4, S5, and S6). Next, we tested whether the intracellular Ca^{2+} chelated sperm can recover motility by bringing extracellular calcium under capacitating conditions. *Efcab9* null sperm took a longer time to recover motility than WT, while *CatSper1* null sperm never recovered (Figures 7C and S7, HTF;Videos S4, S5, and S6). During the intracellular Ca^{2+} chelation, WT sperm beat in both directions albeit with smaller amplitude. *Efcab9* null sperm remained bent at a fixed direction with stiff proximal tails while recovering motility in HTF (Figure S7D; Videos S4, S5, and S6). Altogether, these results indicate that *Efcab9* null spermatozoa have a lower basal level of intracellular calcium and aberrant Ca^{2+} homeostasis. They less efficiently regulate motility, likely due to their combined defects in Ca^{2+} sensing and the altered arrangement of the CatSper channel.

DISCUSSION

EFCAB9 Is a Ca^{2+} Sensor for CatSper Channel and Sperm Motility

Our comparative screen identified many EF-hand containing proteins, which include Centrin1, EFCAB1, EFCAB2, EFCAB3, EFCAB5, EFCAB6, EFCAB9, EFCAB10, EFHB, EFHC2, PLCζ, PPEF1, LETM1, and CaM (Table S1). Among these, only EFCAB9 showed significant change with the loss of CatSper subunits. Because the EF-hand is one of the major Ca^{2+}-binding regions found on many Ca^{2+} sensors, we propose that EFCAB9 is specialized for the CatSper channel. Intriguingly, *Efcab9* is a part of the set of CatSper core genes comprising an evolutionarily conserved unit of flagellar Ca^{2+} channel (Figure S1). In the current study, we report EFCAB9 as a Ca^{2+} sensing auxiliary subunit for the CatSper channel and establish a regulatory mechanism based on the interaction between the EFCAB9-CatSperζ pairs.

Cytoplasmic Ca^{2+} binds directly to channel proteins, or through adaptor or modulatory proteins, to regulate their activity (Clapham, 2007; Yu and Catterall, 2004). Examples of the intrinsic Ca^{2+} sensors include the voltage-gated Ca^{2+} channels, $Ca_v1.2$ (Van Petegem et al., 2005) and the *Arabidopsis thaliana* two pore channel, TPC1 (Guo et al., 2016), as well as RCK-motifs in calcium-regulating BK potassium channels (Piskorowski and Aldrich, 2002). EF-hands are found within the cytoplasmic regions of these channel proteins and alter channel function upon localized Ca^{2+} accumulation. In contrast, the epithelial Ca^{2+} channel, TRPV6 (transient receptor potential vanilloid subfamily member 6) (Singh et al., 2018), the small conductance Ca^{2+} activated K^+ channel, SK (Lee and MacKinnon, 2018), and the subfamily of KCNQ voltage-gated K^+ channels, Kv7.4 (Chang et al., 2018), forms a complex with Ca^{2+} binding protein, CaM, which regulates Ca^{2+}-dependent channel activity. In the CatSper channel, none of the cytoplasmic regions of the nine subunits contains

known Ca^{2+}/CaM binding motifs. Instead, we found that EF1 and/or EF3 of EFCAB9 bind Ca^{2+}. The contribution of individual EF-hands in Ca^{2+}-binding and/or the interaction with CatSperζ will require further investigation.

Before capacitation, EFCAB9-CatSperζ pre-associates with the channel at basal levels of intracellular (~100 nM free) Ca^{2+} (Figures 1G, 3A, and 6A–6E). In this resting state, the channel pore would be mostly closed. Our prediction is that, in the presence of increasing Ca^{2+} concentrations under capacitating conditions, Ca^{2+}-binding to EFCAB9 is likely to cause changes in the structural conformation of EFCAB9, which could affect the interaction with the CatSper channel to control channel activity. The CatSper channel strongly responds to intracellular alkalinization, particularly in the presence of cytosolic free Ca^{2+} (Figures 6A–6F). In the absence of EFCAB9-CatSperζ, the CatSper channel compromises Ca^{2+} sensitivity in the pH-dependent channel activation. Impaired Ca^{2+} sensing leads to inefficient Ca^{2+} uptake through the CatSper channel, demonstrated by the slower kinetics of motility recovery after Ca^{2+} chelation in *Efcab9* null sperm compared to WT sperm (Figures 7C and S7B). Sperm completely lacking CatSper display low bend amplitude and high flagellar beat frequency (Carlson et al., 2005; Marquez et al., 2007; Chung et al., 2011), resembling WT sperm treated to lower intracellular Ca^{2+} (Figure S7D). Moreover, *CatSper* null sperm lose motility significantly over 90 min while WT sperm remain motile (Quill et al., 2003; Qi et al., 2007). Extending the incubation under capacitation led to a further decline in *CatSper1* null sperm motility (Figures 7C). These results suggest that sperm lacking CatSper cannot maintain the basal cytosolic Ca^{2+} because the major Ca^{2+} entry pathway through CatSper is absent, thus lowering cytosolic Ca^{2+} over time. Regardless, the initial motility from WT and *CatSper1* null was comparable (Figures 7C) (Quill et al., 2003; Qi et al., 2007). Intriguingly, *Efcab9* null sperm has lower initial motility than WT and *CatSper1* null sperm but can maintain motility (Figures 7C). These results suggest that *Efcab9* null sperm establish cytosolic basal Ca^{2+} at a lower level than normal, presumably during flagellar development and sperm maturation, due to the presence of functional, albeit less efficient, CatSper. *CatSper1* null sperm are likely to utilize compensatory mechanisms such as activating other Ca^{2+} entry/release pathways and/or inactivating Ca^{2+} clearance pathways.

EFCAB9 Couples pH and Ca^{2+} Sensing

Intracellular pH changes rapidly with sperm in response to the environment; CatSper is activated by intracellular alkalinization in mammals (Kirichok et al., 2006; Lishko et al., 2010, 2011; Miller et al., 2015; Seifert et al., 2015; Strünker et al., 2011) and marine invertebrates (Seifert et al., 2015). This pH-dependent activation of CatSper has been explained through speculation based on amino acid properties and sequence homology. For example, the remarkably histidine-rich amino terminus of CatSper1 subunit has been proposed to sense intracellular pH or bind to Zn^{2+} (Chung et al., 2011; Kirichok et al., 2006). The inability to heterologously express functional CatSper channels has prevented mutagenesis studies from directly testing these ideas. Interestingly, mouse and human CatSper have differential pH sensitivity despite having similar histidine-rich CatSper1 N termini (Miller et al., 2015), and pH changes alone are not enough to gate human CatSper channel (Lishko et al., 2010; Strünker et al., 2011). Indeed, intracellular alkalinization is

sufficient to activate sea urchin CatSper channels (Seifert et al., 2015), despite their lack of a histidine-enriched N terminus. These results suggest that CatSper pH sensing likely utilizes an evolutionarily conserved mechanism.

We hypothesize that, when closed at rest, CatSperζ-complexed EFCAB9 lies near the cytoplasmic mouth of the pore, inhibiting the channel gating by ensuring its closed conformation: pH_i elevation during capacitation partially dissociates EFCAB9 from CatSperζ, which would release gate inhibition and open the pore, enabling EFCAB9 to bind entering Ca^{2+} and undergo a conformational change to maintain the prolonged open state of the channel. Mammalian EFCAB9 couples pH and Ca^{2+} sensing presumably by adopting several substitutions of the functionally important residues in the EF-hands. For example, glutamate at EF-loop position 12 is preserved in all three EF-hands of sea urchin EFCAB9, but replaced by asparagine in EF2 of mammalian EFCAB9. The same position in EF1 is glutamine in mouse EFCAB9, while lysine in human. These changes can contribute to different pH sensitivities between mouse and human CatSper. Likewise, single amino acid substitution of another sperm ion channel also alters sensitivities to both pH and Ca^{2+}. A natural variant (C382R) of SLO3 K^+ channels of human sperm, located between the pore and the cytoplasmic gating ring, has enhanced sensitivities to pH and Ca^{2+} (Geng et al., 2017). Thus, loss of negative charges in mammalian EFCAB9 should lead to a reduction in binding to Ca^{2+} and might affect pH sensitivity of EFCAB9 but presumably enable the interaction with CatSperζ.

The absence of EFCAB9 and/or CatSperζ did not completely eliminate the pH dependence nor the requirement of cytosolic Ca^{2+} for CatSper activation (Figures 6 and S5). Such absence, however, makes the complex much less responsive to alkalinization in the presence of physiologically relevant Ca^{2+}, ultimately making the channel a less efficient Ca^{2+} conductor. Additional molecular determinants could also exist for CatSper pH and Ca^{2+} sensing in mammals. One of the proteins from the proteomic screen contains C2 Ca^{2+} binding domains, providing an avenue for future research. Interestingly, amino acid sequences of CatSperζ are variable among mammals along with the histidine-enriched CatSper1-N termini. It is reasonable to hypothesize that CatSperζ and CatSper1-N termini co-evolved to fine tune variable CatSper pH sensitivity among different mammals. Another potential region is CatSper2's C terminus: mouse CatSper2 has an ~35 amino acid aspartate-rich region, whereas human CatSper2 has an ~80 amino acid serine-rich region. The species-specific features also provide an explanation for the remaining pH sensor components and the different pH sensitivity between mouse and human CatSper channels.

Role of EFCAB9-CatSperζ in CatSper Domain Organization

The two-row structure within a single CatSper quadrant is reminiscent of the previously reported flagellar zipper (Friend and Fawcett, 1974; Selvaraj et al., 2007), but it is uncertain whether the CatSper linear domains are the molecular basis of the zipper structure. Intriguingly, a high-order zipper structure was recently modeled from a quaternary structure of a CatSper tetramer, based on the potential cross-linking ability of the evolutionarily conserved cysteine residues of mammalian CatSper α subunits (Bystroff, 2018). Heterologous reconstitution of the CatSper channel for structural studies remains

at a standstill. Therefore, the possibility of a regularly repeating, quaternary structure of the CatSper complex suggests that direct application of rapidly advancing cryo-EM and cryo-focused ion beam techniques to the sperm tail might be a viable, alternative route for determining molecular details and structure of the CatSper channel. The CatSper complex has multiple transmembrane auxiliary subunits (β, γ, δ, and ε) with large extracellular domains. Any information of the sperm surface nanostructure of CatSper will provide a better understanding of these essential, but otherwise unknown, proteins in functional regulation of CatSper.

Our data illustrate that loss of EFCAB9-CatSperζ results in reduction of the two-row structure to an irregular single structure. While we cannot separate the individual CatSperζ function from EFCAB9, it is reasonable to hypothesize that CatSperζ plays a role in membrane trafficking and scaffolding. CatSperζ might adapt to cytoskeletal structures for the CatSper complex to traffic to the flagellar membrane domains. The fibrous sheath, a cytoskeletal structure of the principal piece unique to the mammalian sperm, lies under the flagellar membrane (Eddy, 2007). Thus, mammalian-specific CatSperζ (Chung et al., 2017) may support the linear arrangement of the CatSper channel complex by linking to an FS component during flagellar development. At the same time, CatSperζ interacts with the pore-forming CatSper α subunits and EFCAB9 (Figures 4, 7, and S6), thus bringing EFCAB9 close to the pore. The CatSper α subunits may form a tetrameric pore via coiled-coil domains in the C terminus (Lobley et al., 2003), leaving the N-terminal domains as candidate EFCAB9-CatSperζ interaction site(s). Surprisingly, neither the purified CatSper1 N- nor C-terminal domain directly bind the EFCAB9-CatSperζ complex or CatSperζ alone. These results suggest that the interaction of EFCAB9-CatSperζ with the pore is not direct between CatSper1 and CatSperζ, but rather complex, probably involving multiple pore subunits. Proteins identified in the comparative proteome screen can serve as a foundation for future studies on the molecular mechanisms governing the coupling between the CatSper domain organization and channel activity.

In summary, we have gained fundamental insights on the regulatory mechanisms of the CatSper channel activity and its domain organization (Figures 7E and 7F). First, we have identified EFCAB9 as an evolutionarily conserved component of the CatSper channel and provided evidence that the EFCAB9-CatSperζ protein pairs are master integrators linking pH- and Ca^{2+} sensing. CatSperζ-complexed EFCAB9 limits Ca^{2+} gating prior to alkalinization but, when pH_i rises, CatSperζ-free EFCAB9 confers pH-dependent activation of CatSper channels. This coordination is achieved by the Ca^{2+}-sensitive and pH-dependent interaction of EFCAB9 and CatSperζ. We further show that EFCAB9-CatSperζ is associated with the channel pore and required for the two-row structure of each single CatSper linear domain, providing a precedent for a linking mechanism for suprastructural domain organization. This study highlights the dual function of EFCAB9-CatSperζ in gatekeeping and domain organization of CatSper.

STAR★METHODS

CONTACT FOR REAGENT AND RESOURCE SHARING

Further information and requests for resources and reagents should be directed to the Lead Contact, Jean-Ju Chung (jean-ju.chung@yale.edu).

EXPERIMENTAL MODEL AND SUBJECT DETAILS

Animals—*CatSper1*, *d*, and *z* null mice generated in the previous studies (Chung et al., 2011, 2017; Ren et al., 2001) are maintained on a C57/BL6 background. Four week old B6D2F1 females for *in vitro* fertilization (IVF) and 7-week-old WT male and female C57BL/6 mice for breeding were purchased from Charles River laboratories. Mice were treated in accordance with guidelines approved by the Yale Animal Care and Use Committees and Boston Children's Hospital (IACUC).

Generation of EFCAB9 null mice by CRISPR/Cas9 and genotyping of mutation: *Efcab9* null mice were generated on a C57BL/6 background using CRISPR/Cas9 system. Female mice were superovulated and mated with males to obtain fertilized eggs. pX330 plasmid expressing guide RNA (5′-CCGCCATGAAACTGACTCCGGGG-3′) targeting the first exon of mouse *Efcab9* was injected into the pronuclei of the fertilized eggs. The developing 2-cell embryos were transplanted into pseudopregnant females. The target region was PCR amplified from alkaline-lysed tail biopsies from founders, and the resulting PCR fragments were subjected to surveyor analysis to examine CRISPR/Cas9 edited indels on the *Efcab9* locus. Monoallelic founders with 5bp or 28bp deletion in the first exon were backcrossed with WT C57/BL6 animals to test germline transmission of the mutant alleles. After the mutant *Efcab9* lines were established, genotyping was performed by multiplex qPCR (*Efcab9*, forward: 5′-GAAAGCTGCCGCCATGAA-3′, reverse: 5′-ACAGTAAGCAGTAGTTTTGTCCAT-3′, and Probe: 5′-(HEX)-CACAGAAAACACCCCGGAGTCAGT-3′; Internal control (IC), forward: 5′-CACGTGGGCTCCAGCATT-3′, reverse: 5′-TCACCAGTCATTTCTGCCTTTG-3′, and Probe: 5′-(TEX615)-CCAATGGTCGGGCACTGCTCAA-3′, BioRad). Potential off-target regions were selected from E-CRISP. Genomic DNA from WT and *Efcab9 null* mice was extracted. Genomic region containing expected off-target sites were amplified and PCR products were sequenced.

Generation of Efcab9;CatSperz null mice: $Efcab9^{-/-}$;$CatSperz^{-/-}$ double knockout mice were generated by mating $Efcab9^{+/-}$ males and $CatSperz^{-/-}$ females. Double knockout mice were obtained by mating between double heterozygous ($Efcab9^{+/-}$;$CatSperz^{+/-}$) males and females. Genotyping was performed by multiplex qPCR (*CatSperz*, forward: 5′-GCCCATCTACACCAACGTAACC-3′, reverse: 5′-AGTAACAACCCGTCGGATTCTC-3′, and Probe: 5′-(Cy5.5)-CGGTCAATCCGCCGTTTGTTC-3′; *Efcab9* and IC primers information as stated for *Efcab9*, BioRad).

Cell Lines

Mammalian cell lines: HEK293T cells (ATTC; derived from female embryonic kidney) were cultured in DMEM (GIBCO) containing 10% FBS (Thermofisher) and 1× Pen/Strep

(GIBCO) at 37°C, 5% CO_2 condition. HEK cells stably expressing human CatSper1 tagged with GFP at C terminus (HEK-hCatSper1-GFP, a kind gift from David Clapham, Janelia/HHMI) were cultured in 1:1 mixture of DMEM and Ham F12 (DMEM/F12) supplemented with 10% FBS, 1× Pen/Strep, and 500 μg/ml concentration of geneticin (G418) (GIBCO).

Bacterial strains: NEB10b (NEB) and BL21-CodonPlus(DE3)-RIL (Agilent Technologies) bacterial strains were used for the molecular cloning and recombinant protein expression, respectively. To express recombinant proteins, freshly formed colonies were picked and inoculated to Luria broth (Sigma-Aldrich) supplemented with 50 μg/ml of chloramphenicol (AmericanBio Inc) and 100 μg/ml of ampicillin (AmericanBio Inc) or 50 μg/ml of kanamycin (AmericanBio Inc) depending on the antibiotic-resistant genes encoded by transformed plasmids. After overnight culture at 37°C, saturated cultivates were inoculated to terrific broth without antibiotics in one to fiftieth ratio (v/v). Protein expression was induced by Isopropyl-1-thio-β-D-galactopyranoside (IPTG) (AmericanBio Inc) when absorbance value of the culture (OD_{600}) reached 0.5 – 0.7. After IPTG induction, cells were cultured at 16°C for 14 – 16hr and harvested to extract recombinant proteins.

Mouse Sperm Preparation and *In Vitro* Capacitation—Epididymal spermatozoa from adult male mice were collected by swim-out from caudal epididymis in M2 medium (EMD Millipore). Collected sperm were incubated in human tubular fluid (HTF) medium (EMD Millipore) at 2×10^6 cells/ml concentration to induce capacitation at 37°C, 5% CO_2 condition for 90 min.

Human Sperm Preparation—Frozen vials of human sperm from healthy, normal male donors were purchased (Fairfax Cryobank). Vials were thawed and mixed with pre-warmed HEPES-buffered saline (HS) (Chung et al., 2017), followed by washing in HS two times. Washed sperm were placed on top of 20% Percoll (Sigma Aldrich) in HS and incubated at 37°C for 30 minutes to allow for motile sperm to swim-into the Percoll layer. After removing the top layer containing immotile fraction, sperm cells with high motility were collected by centrifugation at 2,000 × g and resuspended in HS.

METHOD DETAILS

Antibodies and Reagents—Rabbit polyclonal antibodies specific to mouse CatSper1 (Ren et al., 2001), 2 (Quill et al., 2001), 3, 4 (Qi et al., 2007), β, δ (Chung et al., 2011), and ζ (Chung et al., 2017) were described previously. To produce EFCAB9 antibody recognizing both mouse and human EFCAB9, peptide corresponding to mouse EFCAB9 (137–154, KKQELRDLFHDFDITGDR) was synthesized and conjugated to KLH carrier protein (Open Biosystems). Antisera from the immunized rabbits were affinity-purified using the peptide immobilized Amino Link Plus resin (Pierce). All the other antibodies and reagents used in this study are commercially available and listed in the key resource table. All the chemicals were from Sigma Aldrich unless indicated.

Proteomics Analysis—Whole sperm proteome analysis from WT and *CatSper1* null male mice was performed concomitantly with the previous phosphotyrosine proteome analysis (Chung et al., 2014). In short, sperm cells from WT and *CatSper1* null males (n =

3 per each group) incubated under capacitating conditions were lysed with urea in triplicate. The lysates were reduced, alkylated, trypsin-digested, and reverse-phase purified (Villén and Gygi, 2008). Digested peptides were labeled with TMT to quantify the protein from WT and *CatSper1* null sperm. The labeled peptides were subjected to mass spectrometric analysis using an Orbitrap Fusion mass spectrometer (Thermo Scientific) with an MS^3 method. Tandem mass spectrometry (MS/MS) spectra was matched to peptide using Sequest search engine (Thermo Scientific). Peptides having a total of the TMT reporter ion signal/noise ≥ 65 were quantified. False discovery rate was controlled to 1% at the peptide and protein level.

Open Database Search

Transcriptome database: Gene expression data of *Efcab9*, *Als2cr11*, *Slco6c1*, *Trim69*, and *Fancm* in mouse tissues were obtained from Mouse ENCODE transcriptome data (Yue et al., 2014) as curated in NCBI Gene database.

Genome database: Orthologs of CatSper subunits, EFCAB9, ALS2CR11, SLCO6C1, and TRIM69 proteins in 21 eukaryotes were searched in NCBI gene database or by sequence homology analysis as previously described (Chung et al., 2017). Orthologs not annotated in NCBI gene database were identified by comparing amino acid sequences of human ortholog using BlastP in NCBI (http://blast.ncbi.nlm.nih.gov) or JGI genome portal (https://genome.jgi.doe.gov) with default option. Resulting hits with expected values < 10^{-10} from Blast alignment were considered as orthologs of the query proteins.

Multiple Tissue RT-PCR—PCR was carried out using a commercial multiple cDNA panel (MTC, Clontech). Primer pairs amplifying *Efcab9* (forward: 5′-GAAACGTGAAAGCCTTGATGG-3′ and reverse: 5′-ATCCCGATCTGTGACTTGTTC-3′), *Efcab1* (forward: 5′-GGACAGAGTATTTCGAGGCTTT-3′ and reverse: 5′-GCCATCACCATTCAGATCAAAC-3′), and *Calm1* (forward: 5′-CAACGAAGTGGATGCTGATG-3′ and reverse: 5′-GCACTGATGTAACCATTCCCA-3′) mRNA were used to examine tissue expression of each gene. *Gapdh* (forward: 5′-TGAAGGTCGGTGTGAACGGATTTGGC-3′ and reverse: 5′-ATGTAGGCCATGAGGTCCACCAC-3′) was used for a control.

RNA Extraction, cDNA Synthesis, and Real-Time PCR—Total RNA was extracted from testes of 7, 14, 21, 23, 49, and 80 days old WT males using RNeasy mini-kit (QIAGEN). 500 ng of RNA was used to synthesize cDNAs using iScript cDNA Synthesis (BioRad). cDNAs were used for real-time PCR (CFX96, Biorad) using the primer pairs: *CatSper1* (forward: 5′-CTGCCTCTTCCTCTTCTCTG-3′ and reverse: 5′-TGTCTATGTAGATGAGGGACCA-3′), *CatSperz* (forward: 5′-GAGACCTCCTTAGCATCGTC-3′ and reverse: 5′-TCGTGGACCTATATGTGATGAG-3′), and *18srRNA* (forward: 5′- CGTCTGCCCTATCAACTTTC-3′ and reverse: 5′-GTTTCTCAGGCTCCCTCTCC-3′). Primers described in *Multiple Tissue Expression* were used to amplify *Efcab9*, *Efcab1*, and *Calm1* mRNA. *18srRNA* was used as a reference

gene to normalize quantitative expression by ddCt method. Three sets of experiments were conducted independently.

Molecular cloning

Mammalian cell expression constructs: Mouse *Efcab9* ORF clone (Dharmacon, clone 6771929) was subcloned into phCMV3 (*phCMV3-mEfcab9*) to express mouse EFCAB9 tagged with HA at C terminus. Mouse *CatSperz* (*pCAG-mCatSperz-V5*) (Chung et al., 2017) and *Efcab9* were subcloned into phCMV3 together for bi-cystronic expression (*phCMV3-mCatSperz-V5-p2A-mEfcab9*). Human *Efcab9* ORF (GenScript, #ohu00121d) and *CatSperz* (Chung et al., 2017) were also subcloned into pcDNA3.1 for bi-cystronic expression (pcDNA3.1(−)-*hEfcab9-HA-p2A-hCatSperz-MYC*). Mouse *CatSper1*, *2*, *3*, and *4* (Chung et al., 2014) were subcloned into phCMV3 to express C-terminal Flag-tagged proteins (*phCMV3-mCatSper1, 2, 3, or 4-Flag*). Two ORF clones of human *CatSpere* variants (Dharmacon, clone 5269307 and 4823002) were assembled using NEBuilder® HiFi DNA Assembly (NEB) and cloned into phCMV3 (*phCMV3-Flag-hCatSpere*) for the expression construct of human *CatSpere* CDS (NM_001130957.1). Human CatSperg ORF was subcloned into phCMV3 (*phCMV3-Flag-hCatSperg*). Both human *CatSpere* and *CatSperg* constructs were tagged with Flag at the N-termini. For Flag-tagged CatSper constructs in phCMV3 vector, a stop codon was placed at the upstream of HA sequences.

Bacterial expression constructs—For N-terminal GST-tagged EFCAB9 and 6xHis-tagged CatSperζ expression in bacteria, mouse *Efcab9* and *CatSperz cDNAs* were subcloned into pGEX-6P2 (*pGEX-6P2-mEfcab9*) or pET43.1a(+) (*pET43.1a(+)-mEFCAB9*), and pET32a(+) (*pET32a(+)-gb1-mCatSperz*), respectively. To generate constructs expressing EFCAB9 with two amino acid mutations on EF-hand loops (EFCAB9^{Mut}, D72N/E160Q), *Efcab9* cDNAs were site-directed mutagenized and subcloned into pGEX-6P2 (*pGex-6P2-mEfcab9^{Mut}*) using NEBuilder® HiFi DNA Assembly. The construct to express GST-fused N-terminal intracellular domain of CatSper1 (1–150, *pGEX-2T-mCatSper1-N150*) was a kind gift from D.E. Clapham, Janelia/HHMI. For expression of C-terminal intracellular domain of CatSper1, *pET32a(+)-mCatSper1-C-Flag* was constructed by amplifying a fragment of *CatSper1* cDNA encoding amino acids 574–686 tagged with Flag at C terminus.

Recombinant protein expression in mammalian cells—HEK293T cells were transiently transfected with plasmids encoding various CatSper subunits in combination: the pore-forming (mouse CatSper1, 2, 3, and 4) or the auxiliary (mouse CatSperβ, δ, ζ, EFCAB9, human CatSperγ, ε, or mouse and human CatSperζ and EFCAB9 bi-cystronically) subunits. HEK cells stably expressing GFP-tagged human CatSper1 at C terminus were transfected with a plasmid encoding human CatSperζ and human EFCAB9 bi-cistronically. Lipofectamin 2000 (Invitrogen) or polyethyleneimine (PEI) reagent were used for transfection following the manufacturer's instruction. Transfected cells were used to characterize antibodies or co-immunoprecipitation (coIP) experiments.

Protein Extraction, Immunoprecipitation, and western blotting

Preparation and solubilization of testis microsome: Mouse testes were homogenized in 0.32M sucrose at 1:10 (wt/vol), and cell debris and nuclei were removed by centrifugation at

1,000 × g, 4°C for 10 min. Supernatant was centrifuged at 105,000 × g for 60 min at 4°C to collect membrane preparation (microsome). The microsome fraction was solubilized in 1% Triton X-100 in PBS (4 mg/ml) with protease inhibitor cocktail (complete mini, Roche) by rocking at 4°C for 60 min. The lysate was cleared by centrifugation at 14,000 × g, 4°C for 30 min to obtain soluble (supernatant, S) and insoluble (pellet, P) fractions. Protein samples volume equivalent from S and P fractions were subjected to SDS-APGE and immunoblot to examine the partitioning of proteins.

Preparation of whole sperm lysate and solubilized protein extracts: Whole sperm protein from mouse and human sperm was extracted as previously described (Chung et al., 2011, 2014, 2017). In short, mouse epididymal spermatozoa washed in PBS were directly lysed in 2X SDS sample buffer. Washed motile human sperm from cryopreserved vials (Fairfax Cryobank) were lysed in PBS containing 0.1% SDS, 0.5% sodium deoxycholate, 1 mM DTT, 1 mM EDTA and protease inhibitors by sonication. The whole sperm lysates were centrifuged at 15,000 × g, 4°C for 10 min. After adjusting DTT to 50 mM, supernatant was denatured at 75°C for 10 min before loading to gel. To test the partitioning of proteins into soluble (S) and insoluble (P) fractions, mouse sperm cells were sonicated briefly in 1% Triton X-100 in PBS with protease inhibitor, further extracted for 60 min at 4°C, and cleared by centrifugation at 10,000 × g for 30 min (Chung et al., 2014). Volume equivalent protein samples from S and P fractions were subjected to SDS-PAGE.

Immunoprecipitation from transfected 293T cells: Transfected HEK293T cells and HEK cells expressing GFP-tagged human CatSper1 were lysed with 1% Triton X-100 in PBS containing EDTA-free protease inhibitor cocktail (Roche) by rocking at 4°C for 1 hr, and centrifuged at 14,000 × g for 30 minutes at 4°C. Solubilized proteins in the supernatant were mixed with Protein A/G-magnetic beads conjugated with either 1 μg each of rabbit polyclonal antibodies (GFP (FL, SantaCruz), mouse CatSper1, mouse CatSperδ, mouse CatSperζ, human CatSperζ) or mouse monoclonal antibodies (Flag (clone M2, Sigma-Aldrich), MYC (9E10, SantaCruz), HA magnetic beads (clone 2–2.2.14, Pierce)) or V5 agarose (clone V5–10, Sigma-Aldrich). The immune complexes were incubated at 4°C overnight and coIP products were eluted with 60 mL of 2× LDS sampling buffer supplemented with 50 μM dithiothreitol (DTT) and denatured at 75°C for 10 minutes. Primary antibodies used for the western blotting were: rabbit polyclonal anti-mouse CatSper1, CatSper2, CatSper3, CatSper4, CatSperβ, CatSperδ, EFCAB9, human CatSperζ, GFP (FL, SantaCruz), CaM, (05–173, Upstate), phosphotyrosine (clone 4G10, EMD Millipore) at 1 μg/ml, mouse CatSperζ (2.7 μg/ml), mouse monoclonal anti-PMCA4 (clone JA9, Novus) at 1 μg/ml anti-HA (clone 2–2.2.14, Pierce), Flag (clone M2, Sigma-Aldrich) at 0.5 μg/ml, acetylated tubulin (T7451, Sigma Aldrich, 1:20,000), HRP-conjugated V5 (clone E10/V4RR, ThermoFisher, 1:2,000), HA (clone 6E2, CST, 1:1,000), and MYC (Clone 9B11, CST, 1:1,000). For secondary antibodies, anti-mouse IgG-HRP, anti-rabbit IgG-HRP (Jackson ImmunoResearch, 1:10,000) and mouse IgG Trueblot (clone eB144, Rockland, 1:1,000) were used.

Sperm Immunocytochemistry—Mouse and human sperm were washed in PBS twice, attached on the glass coverslips, and fixed with 4% paraformaldehyde (PFA) in PBS at

room temperature (RT) for 10 minutes (mouse) or at 4°C for 1 hr (human). Fixed samples were permeabilized using 0.1% Triton X-100 in PBS at RT for 10 minutes, washed in PBS, and blocked with 10% goat serum in PBS at RT for 1 hr. Cells were stained with anti-mouse EFCAB9 (20 μg/ml), CatSper1 (10 μg/ml), or CatSperζ (20 μg/ml) in PBS supplemented with 10% goat serum at 4°C overnight. After washing in PBS, the samples were incubated with goat anti-rabbit Alexa647 or Alexa555-plus (Invitrogen, 1:1,000) in 10% goat serum in PBS at RT for 1 hr. Immunostained samples were mounted with Prolong gold (Invitrogen) and cured for 24 hr, followed by imaging with Zeiss LSM710 Elyra P1 using Plan-Apochrombat 63X/1.40 and alpha Plan-APO 100X/1.46 oil objective lens (Carl Zeiss). Hoechst dye was used to counterstain nucleus for sperm head.

Super-Resolution Imaging

Structured illumination microscopy: Structured illumination microscopy (SIM) imaging was performed with Zeiss LSM710 Elyra P1 using alpha Plan-APO 100X/1.46 oil objective lens. Samples were prepared as described in Sperm Immunocytochemistry with a minor modification in that the immunostained sperm coverslips were mounted with VectaSheild (Vector laboratory). 2D SIM images were taken using a laser at 642 nm (150 mW) for Alexa647 (Invitrogen). The images were acquired using 5 grid rotations with a 51 nm SIM grating period. For 3D SIM images, a laser at 561nm (200 mW) was used for Alexa 555-plus (Invitrogen). Z stack was acquired from 42 optical sections with a 100 nm interval. Each section was imaged using 5 rotations with a 51 nm grating period. Both 2D and 3D SIM Images were rendered using Zen 2012 SP2 software.

4Pi Single-Molecule Switching Nanoscopy: Mouse sperm were attached onto the center of 25-mm diameter of glass coverslips. The samples were prepared as described in Sperm immunocytochemistry with Alexa647-conjugated 2nd antibody. The samples were imaged with a custom-built 4Pi Single-Molecule Switching Nanoscopy (4Pi-SMSN) system as previously described (Huang et al., 2016) with minor modifications. Briefly, the fluorescent signal was collected coherently by two opposing objectives (100 ×/1.35NA, silicone oil immersion, Olympus) and imaged on a sCMOS camera (ORCA-Flash 4.0v2, Hamamatsu). The microscope was equipped with an excitation laser at 642 nm (MPB Communications, 2RU-VFL-2000–642-B1R) and an activation laser at 405 nm (Coherent OBIS 405 LX, 50 mW). All data were acquired at 100 fps at a 642 nm laser intensity of about 7.5 kW/cm^2. The full system design and the image analysis algorithms were previously described in detail (Huang et al., 2016). The 4Pi movies were rendered using Vutara SRX software (Bruker). Angular profiling was carried out as previously reported (Chung et al., 2014).

Scanning Electron Microscopy—Sperm from WT, *CatSper1 null*, and *Efcab9 null* males were washed in PBS and attached on the glass coverslips. The coverslips were fixed with 4% paraformaldehyde in PBS for 10 minutes at RT, and washed in PBS twice. The coverslips were incubated with 2.5% glutaraldehyde in 0.1M sodium cacodylate buffer pH7.4 for another hour at 4°C. Samples were then rinsed, post fixed in 2% osmium tetroxide in 0.1M sodium cacodylate buffer pH 7.4, and dehydrated through a series of ethanol to 100%. The samples were dried using a Leica 300 critical point dryer with liquid carbon

dioxide as transitional fluid. The coverslips were glued to aluminum stubs, and sputter coated with 5 nm platinum using a Cressington 208HR (Ted Pella) rotary sputter coater.

Mating Test and *In Vitro* Fertilization—Female mice were caged with heterozygous or homozygous *Efcab9* mutant or *Efcab9*; *CatSperz* double mutant males for two months to record pregnancy and litter size when gave births. For IVF, 5 –7 weeks B6D2F1 female mice were superovulated by injecting progesterone and anti-inhibin serum (Central Research Co, Ltd) (Hasegawa et al., 2016), and the oocytes were collected after injecting 13 hr from 5 U of human chorionic gonadotrophin (EMD millipore). Prepared epididymal sperm were capacitated at 37°C for 90 min, and inseminated to oocytes with 2×10^5 cells/ml concentration. After 5 hr co-incubation, oocytes were washed and transferred to fresh HTF medium, and cultured overnight at 37°C under 5% CO_2. 2-cell embryos were counted 20–22 h after insemination as successful fertilization.

Flagella Waveform Analysis—To tether sperm head for planar beating, non-capacitated or capacitated spermatozoa (2×10^5 cells) from adult male mice were transferred to the fibronectin-coated 37°C chamber for Delta T culture dish controller (Bioptechs) filled with HEPES-buffered HTF medium (H-HTF) (Chung et al., 2017) for 1 minute. Flagellar movements of the tethered sperm were recorded for 2 s with 200 fps using pco.edge sCMOS camera equipped in Axio observer Z1 microscope (Carl Zeiss). All movies were taken at 37°C within 10 minutes after transferring sperm to the imaging dish. FIJI software (Schindelin et al., 2012) was used to measure beating frequency and α-angle of sperm tail, and to generate overlaid images to trace waveform of sperm flagella as previously described (Chung et al., 2017).

Recombinant Protein Purification—Each construct expressing GST-tagged $EFCAB9^{WT}$, $EFCAB9^{Mut}$, and N terminus of CatSper1 (CatSper-N150) and 6xHis-tagged CatSperζ and C terminus of CatSper1 (CatSper1-C) was transformed to BL21-CodonPlus(DE3)-RIL competent cells (Agilent Technologies). Fresh colonies were inoculated and cultured into LB with antibiotics at 37°C overnight. Saturated cultivates were 50 times diluted in TB medium and cultured further at 37°C until the OD_{600} values reach 0.5 – 0.7. To induce protein expression, IPTG (0.2mM for EFCAB9 and CatSper1-N150; 0.1 mM for CatSperζ; 0.05 mM for $EFCAB9^{Mut}$ and CatSper1-C) was added to the bacteria cultures and incubated further for 16 hr at 16°C. When the CatSper1-N150 recombinant protein expression is induced by IPTG, proteasome inhibitor MG-132 (Calbiochem) was added to 10 μM. Cultured cells were harvested and washed with cold PBS. Cell pellets were resuspended in buffers containing 10 mM HEPES in pH 8.0 ($EFCAB9^{WT}$ and $EFCAB9^{Mut}$), pH 7.5 (CatSper1-N150 and CatSper1-C) or pH6.0 (CatSperζ) with 135 mM NaCl containing EDTA-free protease inhibitor cocktail (Roche). MG-132 was also added to 30 μM in the resuspension buffer for CatSper1-N150 recombinant protein purification. Resuspended cells were lysed using EmulsiFlex-C3 (AVESTIN, Inc.) or VCX500 sonicator (SONICS). Lysates were centrifuged at 14,000 × g for 1 hr at 4°C. The supernatant were incubated with glutathione agarose (Pierce) or HisPur Ni-NTA resin (Pierce) depending on the tag of the target recombinant proteins for 1 hr at RT. Glutathione agarose was washed with 10 mM HEPES buffer pH7.5, 140 mM NaCl and the GST-fused protein was eluted

in the elution buffer (50 mM HEPES buffer pH7.4 with 10 mM reduced glutathione). Ni-NTA resin was washed with 10 mM HEPES buffer pH6.5, 300 mM NaCl with 30 mM (CatSper1-C) or 100 mM (CatSperζ) Imidazole and the His-tagged proteins were eluted with the buffer containing 10 mM HEPES buffer pH7.4, 135 mM NaCl, 300 mM Imidazole. The eluents were dialyzed at 4°C against storage buffer (10mM HEPES buffer pH7.4, 135mM NaCl in 50% glycerol). To express and purify recombinant EFCAB9 and CatSperζ proteins together, competent cells were transformed by *pET43.1a(+)-mEfcab9* and *pET32a(+)-mCatSperz* together. A fresh colony was picked and cultured as described above. To induce the protein expression, the cells were treated with 0.05 mM IPTG and harvested after 14 hr culture at 16°C. After washing in PBS, the pellet was resuspended in 10 mM HEPES buffer pH7.5, 150 mM NaCl, and lysed using EmulsiFlex-C3 (AVESTIN, Inc.). Lysates were centrifuged and the collected supernatant was incubated with glutathione agarose. The agarose was washed with 10 mM HEPES buffer pH7.5, 150 mM NaCl. The bound recombinant proteins were eluted from the glutathione agarose with the elution buffer for GST-tagged protein, followed by dialysis against the storage buffer as described above.

Pull-down Assay—Pull-down assay was performed to test direct binding between purified recombinant proteins. 5 μL of glutathione agarose (GST pull-down; Pierce), HisPur Ni-NTA resin (His pull-down; Pierce), or 15 ul of Protein-A/G agarose beads slurry (SantaCruz) cross-linked with CatSper1 antibody was equilibrated with pre-binding buffer (10 mM HEPES pH7.5, 140 mM NaCl), and incubated with the recombinant GST-tagged EFCAB9 or 6xHis tagged CatSperζ, or GST-CatSper1-N150 protein (bait proteins), respectively, at 4°C for overnight. Incubated resin was washed in pre-binding buffer three times and equilibrated in the binding buffer in various compositions for each experiment. Prey proteins subjected to interact with bait proteins were incubated with the resin equilibrated with binding buffer for 1 hr at RT. The resin was washed in the binding buffer for each group four times. Resin was collected and the bound proteins were eluted with 2X LDS sampling buffer supplemented with 50 mM DTT, and denatured at 75°C for 10 minutes. Protein interaction was confirmed by Coomassie blue staining (GelCode^{Tm} Blue Safe Protein Satin, ThermoFisher) or western blotting. Detailed experiment procedures and compositions of binding buffers for each experiment are as described below.

Interaction between EFCAB9 and CatSperζ: Recombinant EFCAB9 and CatSperζ proteins were used as bait for glutathione agarose or His-Pur Ni-NTA resin, respectively to test their interaction reciprocally. In His-pull down assay, pre-binding buffer contains 30 mM Imidazole. Each pre-binding buffer used in GST or His pull-down assay was also used as binding buffer.

Ca^{2+}- or pH-dependent interaction between EFCAB9 and CatSperζ: To examine the Ca^{2+}- or pH-sensitivity of the interaction, GST pull-down was performed with the recombinant proteins. Recombinant EFCAB9 bound to glutathione resin was equilibrated with binding buffer at pH7.5 with different Ca^{2+} concentration by adding 2 mM $CaCl_2$ or 2 mM EGTA or different pH (pH 6.0, 7.5, and 8.5) with nominal 0 Ca^{2+} concentration (no added Ca^{2+}). Calcium and pH-dependent interaction within mutated EFCAB9 and CatSperζ recombinant proteins was examined with the same buffers.

Interaction between EFCAB9-CatSperζ complex and CatSper1 intracellular domains: Co-purified EFCAB9-CatSperζ recombinant proteins were subjected to interact with either N- or C-terminal domain of CatSper1 protein purified as described. Direct interaction of N-terminal domain (CatSper1-N150) with CatSperζ or EFCAB9-CatSperζ complex was tested by pulling down CatSper1-N150 with glutathione agarose or CatSper1-crosslinked A/G agarose slurry beads. GST pull-down was performed to test the interaction between EFCAB9-CatSperζ complex and CatSper1-C.

Sequence comparison of orthologs—Protein sequences of EFCAB9, CatSperζ, and intracellular domains of CatSper1, 2, 3, 4 and $Ca_V3.1$ over 100 amino-acid residues were collected from 12 mammals, mouse (*Mus musculus*), rat (*Rattus norvegicus*), hamster (*Cricetulus griseus*), squirrel (*Ictidomys tridecemlineatus*), human (*Homo sapiens*), chimpanzee (*Pan troglodytes*), baboon (*Papio anubis*), pig (*Sus scrofa*), cow (*Bos taurus*), dog (*Canis lupus familiaris*), cat (*Felis catus*), and ferret (*Mustela putorius furo*). Ortholog sequences were aligned by MUSCLE alignment algorithm with default option (Edgar, 2004), and pairwise distances between orthologs were calculated. Pairwise distances were represented to heatmaps indicating sequence diversity among mammals.

Electrophysiology—Sperm cells from adult male mice were allowed to adhere to glass coverslips. Gigaohm seals were formed at the cytoplasmic droplet of motile sperm cells in standard HEPES saline buffer containing (in mM): 130 NaCl, 20 HEPES, 10 lactic acid, 5 glucose, 5 KCl, 2 $CaCl_2$, 1 MgSO4, 1 sodium pyruvate, pH 7.4 adjusted with NaOH, 320 mOsm/L (Lishko et al., 2011, 2010). Transition into whole-cell mode was achieved by applying voltage pulses (400–620 mV, 1 ms) and simultaneous suction. Data were sampled at 10 Hz and filtered at 1 kHz and cells were stimulated every 5 s. The divalent-free bath solution (DVF, ~320 mOsm/L) consisted of (in mM): 140 $CsMeSO_3$, 40 HEPES, 1 EDTA and pH 7.4 was adjusted with CsOH. pH-dependent $I_{CatSper}$ from WT and *CatSperz* null sperm recorded with pipette solution (~335 mOsm/L) contained (in mM): 130 $CsMeSO_3$, 60 MES, 3 EGTA, 2 EDTA, 0.5 Tris-HCl. Access resistance was 43–62 MU. To induce intracellular alkalization (pH_i = ~7.4), 10 mM NH_4Cl were added to the bath solution. For experiments with defined intracellular pH and 0 μM, 0.1 μM, or 10 μM Ca^{2+}, inside pipette solution containing (in mM):130 $CsMeSO_3$, 60 MES (pH = 6.0) or 60 HEPES (pH = 7.4), 4 CsCl, 5 EGTA, and 2 EDTA (0 μM Ca^{2+}), 130 $CsMeSO_3$, 65 MES (pH = 6.0) or 65 HEPES (pH = 7.4), 4 CsCl, 1 EGTA, 1 EDTA, and 1 BAPTA (0.1 μM Ca^{2+}) or 130 $CsMeSO_3$, 65 MES (pH = 6.0) or 60 HEPES (pH = 7.4), 4 CsCl and 2 HEDTA (10 μM Ca^{2+}). Required $CaCl_2$ for desired free Ca^{2+} concentration was calculated with WinMAXC32 version 2.51 (Chris Patton, Stanford University). Access resistance was 42–61 MΩ. pH of pipette solution was adjusted with CsOH. All experiments were performed at 22°C. Data were analyzed with Clampfit (v10.3, pClamp) and OriginPro (v9.0, Originlab).

Analyses of sperm motility during intracellular Ca^{2+} removal and recovery

Sample preparation: Epididymal sperm from WT, *CatSper1* null, and *Efcab9* null males were collected in M2 medium by swim-out. Sperm (3.5×10^6 cells/ml) were loaded with 5 μM BAPTA-AM (bis-(o-aminophenoxy)ethane-*N*,*N*,*N*′,*N*′-tetra-acetic acid acetoxymethyl ester), the membrane-permeable Ca^{2+} chelator, for 90 min at 37°C in M2 to buffer

intracellular Ca^{2+} or vehicle (0.05% DMSO and 0.01% F-127). Extracellular BAPTA-AM was removed by centrifugation of the sperm suspension at 700 × g for 2.5 min twice with modified H-HTF medium without $CaCl_2$, $NaHCO_3$, and BSA (in mM): 92 NaCl, 4.7 KCl, 0.2 $MgCl_2$, 0.37 KH_2PO_4, 2.78 glucose, 0.33 sodium pyruvate, 18.3 sodium lactate, 10 HEPES and pH7.4 adjusted with NaOH. Washed sperm pellets were incubated in normal HTF with 2 mM $CaCl_2$ for restoring intracellular Ca^{2+} under capacitating conditions at 37°C with 5% CO_2 for 90 min.

Motility analysis—Aliquots of sperm were placed in slide chamber (CellVision, 20 μm depth) and motility was examined on a 37°C stage of a Nikon E200 microscope under 10× phase contrast objective (CFI Plan Achro 10X/0.25 Ph1 BM, Nikon). Images were recorded (40 frames at 50 fps) using CMOS video camera (Basler acA1300–200um, Basler AG, Ahrensburg, Germany) and analyzed by computer-assisted sperm analysis (CASA, Sperm Class Analyzer version 6.3, Microptic, Barcelona, Spain). Sperm motility (%) was quantified, and motion parameters including curvilinear velocity (VCL, in μm/s) and amplitude of lateral head displacement (ALH, in μM) were measured. For each time point, over 200 motile sperm were analyzed and for each experiment, replicate tests were performed using three (*Efcab9*$^{-/-}$) to four (WT and *CatSper1*$^{-/-}$) males from each genotype. For flagella waveform analysis, sperm loaded with BAPTA-AM or vehicle in M2 were imaged in the same medium. Sperm during recovery from BAPTA-AM were imaged in H-HTF. Movies were taken at 200 fps for 2 s and overlaid images from two beat cycles were generated by ImageJ.

QUANTIFICATION AND STATISTICAL ANALYSIS

Statistical analyses were performed using Student's t test or one-way analysis of variance (ANOVA) with Tukey post hoc test. Differences were considered significant at *$p < 0.05$, **$p < 0.01$, and ***$p < 0.001$. Pairwise distances between orthologs were calculated using MEGA6 software (Tamura et al., 2013).

DATA AND SOFTWARE AVAILABILITY

The raw images of immunoblot in this study are available on Mendeley Data at https://doi.org/10.17632/mv52ykks6x.1. All software used in this study is listed in the Key Resources Table.

Supplementary Material

Refer to Web version on PubMed Central for supplementary material.

ACKNOWLEDGMENTS

We thank David E. Clapham for sharing reagents, Sang-Hee Shim for sharing algorithm for angular plots, Jong-Nam Oh for assistance in immunocytochemistry with human sperm samples and solubility test of native proteins, and the Yale Center for Cellular and Molecular Imaging for assistance in scanning electron microscopy. This work was supported by start-up funds from Yale University School of Medicine, a Yale Goodman-Gilman Scholar Award-2015, and a Rudolf J. Anderson Fellowship award to J.-J.C.; by NIH (R01GM111802), Pew Biomedical Scholars and Rose Hill awards, and Packer Wentz Endowment Will to P.V.L.; and by the Wellcome Trust (203285/B/16/Z) and the Yale Diabetes Research Center (NIH P30 DK045735) to J.B.

REFERENCES

Avenarius MR, Hildebrand MS, Zhang Y, Meyer NC, Smith LL, Kahrizi K, Najmabadi H, and Smith RJ (2009). Human male infertility caused by mutations in the CATSPER1 channel protein. Am. J. Hum. Genet. 84, 505–510. [PubMed: 19344877]

Böhmer M, Van Q, Weyand I, Hagen V, Beyermann M, Matsumoto M, Hoshi M, Hildebrand E, and Kaupp UB (2005). Ca2+ spikes in the flagellum control chemotactic behavior of sperm. EMBO J. 24, 2741–2752. [PubMed: 16001082]

Brown SG, Miller MR, Lishko PV, Lester DH, Publicover SJ, Barratt CLR, and Martins Da Silva S. (2018). Homozygous in-frame deletion in CATSPERE in a man producing spermatozoa with loss of CatSper function and compromised fertilizing capacity. Hum. Reprod. 33, 1812–1816. [PubMed: 30239785]

Bystroff C (2018). Intramembranal disulfide cross-linking elucidates the super-quaternary structure of mammalian CatSpers. Reprod. Biol. 18, 76–82. [PubMed: 29371110]

Carlson AE, Westenbroek RE, Quill T, Ren D, Clapham DE, Hille B, Garbers DL, and Babcock DF (2003). CatSper1 required for evoked Ca2+ entry and control of flagellar function in sperm. Proc. Natl. Acad. Sci. USA 100, 14864–14868. [PubMed: 14657352]

Carlson AE, Quill TA, Westenbroek RE, Schuh SM, Hille B, and Babcock DF (2005). Identical phenotypes of CatSper1 and CatSper2 null sperm. J. Biol. Chem. 280, 32238–32244. [PubMed: 16036917]

Castaneda JM, Hua R, Miyata H, Oji A, Guo Y, Cheng Y, Zhou T, Guo X, Cui Y, Shen B, et al. (2017). TCTE1 is a conserved component of the dynein regulatory complex and is required for motility and metabolism in mouse spermatozoa. Proc. Natl. Acad. Sci. USA 114, E5370–E5378. [PubMed: 28630322]

Catterall WA (2011). Voltage-gated calcium channels. Cold Spring Harb. Perspect. Biol. 3, a003947. [PubMed: 21746798]

Chang H, and Suarez SS (2011). Two distinct Ca(2+) signaling pathways modulate sperm flagellar beating patterns in mice. Biol. Reprod. 85, 296–305. [PubMed: 21389347]

Chang A, Abderemane-Ali F, Hura GL, Rossen ND, Gate RE, and Minor DL Jr. (2018). A Calmodulin C-Lobe Ca(2+)-Dependent Switch Governs Kv7 Channel Function. Neuron 97, 836–852. [PubMed: 29429937]

Chung JJ, Navarro B, Krapivinsky G, Krapivinsky L, and Clapham DE (2011). A novel gene required for male fertility and functional CATSPER channel formation in spermatozoa. Nat. Commun. 2, 153. [PubMed: 21224844]

Chung JJ, Shim SH, Everley RA, Gygi SP, Zhuang X, and Clapham DE (2014). Structurally distinct Ca(2+) signaling domains of sperm flagella orchestrate tyrosine phosphorylation and motility. Cell 157, 808–822. [PubMed: 24813608]

Chung JJ, Miki K, Kim D, Shim SH, Shi HF, Hwang JY, Cai X, Iseri Y, Zhuang X, and Clapham DE (2017). CatSperzeta regulates the structural continuity of sperm Ca(2+) signaling domains and is required for normal fertility. eLife 6, e23082. [PubMed: 28226241]

Clapham DE (2007). Calcium signaling. Cell 131, 1047–1058. [PubMed: 18083096]

Eddy EM (2007). The scaffold role of the fibrous sheath. Soc. Reprod. Fertil. Suppl. 65, 45–62. [PubMed: 17644954]

Edgar RC (2004). MUSCLE: multiple sequence alignment with high accuracy and high throughput. Nucleic Acids Res. 32, 1792–1797. [PubMed: 15034147]

Friend DS, and Fawcett DW (1974). Membrane differentiations in freeze-fractured mammalian sperm. J. Cell Biol. 63, 641–664. [PubMed: 4423603]

Geng Y, Ferreira JJ, Dzikunu V, Butler A, Lybaert P, Yuan P, Magleby KL, Salkoff L, and Santi CM (2017). A genetic variant of the sperm-specific SLO3 K^+ channel has altered pH and Ca^{2+} sensitivities. J. Biol. Chem. 292, 8978–8987. [PubMed: 28377504]

Guo J, Zeng W, Chen Q, Lee C, Chen L, Yang Y, Cang C, Ren D, and Jiang Y (2016). Structure of the voltage-gated two-pore channel TPC1 from Arabidopsis thaliana. Nature 531, 196–201. [PubMed: 26689363]

Hasegawa A, Mochida K, Inoue H, Noda Y, Endo T, Watanabe G, and Ogura A (2016). High-yield superovulation in adult mice by anti-inhibin serum treatment combined with estrous cycle synchronization. Biol. Reprod. 94, 21. [PubMed: 26632610]

Hildebrand MS, Avenarius MR, Fellous M, Zhang Y, Meyer NC, Auer J, Serres C, Kahrizi K, Najmabadi H, Beckmann JS, and Smith RJ (2010). Genetic male infertility and mutation of CATSPER ion channels. Eur. J. Hum. Genet. 18, 1178–1184. [PubMed: 20648059]

Ho HC, and Suarez SS (2001). An inositol 1,4,5-trisphosphate receptor-gated intracellular Ca(2+) store is involved in regulating sperm hyperactivated motility. Biol. Reprod. 65, 1606–1615. [PubMed: 11673282]

Huang F, Sirinakis G, Allgeyer ES, Schroeder LK, Duim WC, Kromann EB, Phan T, Rivera-Molina FE, Myers JR, Irnov I, et al. (2016). Ultra-High Resolution 3D Imaging of Whole Cells. Cell 166, 1028–1040. [PubMed: 27397506]

Ishijima S, Baba SA, Mohri H, and Suarez SS (2002). Quantitative analysis of flagellar movement in hyperactivated and acrosome-reacted golden hamster spermatozoa. Mol. Reprod. Dev. 61, 376–384. [PubMed: 11835583]

Kirichok Y, Navarro B, and Clapham DE (2006). Whole-cell patch-clamp measurements of spermatozoa reveal an alkaline-activated Ca2+ channel. Nature 439, 737–740. [PubMed: 16467839]

Lee CH, and MacKinnon R (2018). Activation mechanism of a human SK-calmodulin channel complex elucidated by cryo-EM structures. Science 360, 508–513. [PubMed: 29724949]

Lishko PV, Botchkina IL, Fedorenko A, and Kirichok Y (2010). Acid extrusion from human spermatozoa is mediated by flagellar voltage-gated proton channel. Cell 140, 327–337. [PubMed: 20144758]

Lishko PV, Botchkina IL, and Kirichok Y (2011). Progesterone activates the principal Ca2+ channel of human sperm. Nature 471, 387–391. [PubMed: 21412339]

Liu J, Xia J, Cho KH, Clapham DE, and Ren D (2007). CatSperbeta, a novel transmembrane protein in the CatSper channel complex. J. Biol. Chem. 282, 18945–18952. [PubMed: 17478420]

Lobley A, Pierron V, Reynolds L, Allen L, and Michalovich D (2003). Identification of human and mouse CatSper3 and CatSper4 genes: characterisation of a common interaction domain and evidence for expression in testis. Reprod. Biol. Endocrinol. 1, 53. [PubMed: 12932298]

Luo T, Chen HY, Zou QX, Wang T, Cheng YM, Wang HF, Wang F, Jin ZL, Chen Y, Weng SQ, and Zeng XH (2019). A novel copy number variation in CATSPER2 causes idiopathic male infertility with normal semen parameters. Hum. Reprod. 34, 414–423. [PubMed: 30629171]

Marquez B, Ignotz G, and Suarez SS (2007). Contributions of extracellular and intracellular Ca2+ to regulation of sperm motility: Release of intracellular stores can hyperactivate CatSper1 and CatSper2 null sperm. Dev. Biol. 303, 214–221. [PubMed: 17174296]

Miller MR, Mansell SA, Meyers SA, and Lishko PV (2015). Flagellar ion channels of sperm: similarities and differences between species. Cell Calcium 58, 105–113. [PubMed: 25465894]

Miller MR, Mannowetz N, Iavarone AT, Safavi R, Gracheva EO, Smith JF, Hill RZ, Bautista DM, Kirichok Y, and Lishko PV (2016). Unconventional endocannabinoid signaling governs sperm activation via the sex hormone progesterone. Science 352, 555–559. [PubMed: 26989199]

Miller MR, Kenny SJ, Mannowetz N, Mansell SA, Wojcik M, Mendoza S, Zucker RS, Xu K, and Lishko PV (2018). Asymmetrically Positioned Flagellar Control Units Regulate Human Sperm Rotation. Cell Rep. 24, 2606–2613. [PubMed: 30184496]

Naraghi M, and Neher E (1997). Linearized buffered Ca2+ diffusion in microdomains and its implications for calculation of [Ca2+] at the mouth of a calcium channel. J. Neurosci. 17, 6961–6973. [PubMed: 9278532]

Navarrete FA, García-Vázquez FA, Alvau A, Escoffier J, Krapf D, Sánchez-Cárdenas C, Salicioni AM, Darszon A, and Visconti PE (2015). Biphasic role of calcium in mouse sperm capacitation signaling pathways. J. Cell. Physiol. 230, 1758–1769. [PubMed: 25597298]

Piskorowski R, and Aldrich RW (2002). Calcium activation of BK(Ca) potassium channels lacking the calcium bowl and RCK domains. Nature 420, 499–502. [PubMed: 12466841]

Qi H, Moran MM, Navarro B, Chong JA, Krapivinsky G, Krapivinsky L, Kirichok Y, Ramsey IS, Quill TA, and Clapham DE (2007). All four CatSper ion channel proteins are required for male fertility

and sperm cell hyperactivated motility. Proc. Natl. Acad. Sci. USA 104, 1219–1223. [PubMed: 17227845]

Quill TA, Ren D, Clapham DE, and Garbers DL (2001). A voltage-gated ion channel expressed specifically in spermatozoa. Proc. Natl. Acad. Sci. USA 98, 12527–12531. [PubMed: 11675491]

Quill TA, Sugden SA, Rossi KL, Doolittle LK, Hammer RE, and Garbers DL (2003). Hyperactivated sperm motility driven by CatSper2 is required for fertilization. Proc. Natl. Acad. Sci. USA 100, 14869–14874. [PubMed: 14657366]

Ren D, Navarro B, Perez G, Jackson AC, Hsu S, Shi Q, Tilly JL, and Clapham DE (2001). A sperm ion channel required for sperm motility and male fertility. Nature 413, 603–609. [PubMed: 11595941]

Schindelin J, Arganda-Carreras I, Frise E, Kaynig V, Longair M, Pietzsch T, Preibisch S, Rueden C, Saalfeld S, Schmid B, et al. (2012). Fiji: an open-source platform for biological-image analysis. Nat. Methods 9, 676–682. [PubMed: 22743772]

Seifert R, Flick M, Bönigk W, Alvarez L, Trötschel C, Poetsch A, Müller A, Goodwin N, Pelzer P, Kashikar ND, et al. (2015). The CatSper channel controls chemosensation in sea urchin sperm. EMBO J. 34, 379–392. [PubMed: 25535245]

Selvaraj V, Asano A, Buttke DE, McElwee JL, Nelson JL, Wolff CA, Merdiushev T, Fornés MW, Cohen AW, Lisanti MP, et al. (2006). Segregation of micron-scale membrane sub-domains in live murine sperm. J. Cell. Physiol. 206, 636–646. [PubMed: 16222699]

Selvaraj V, Buttke DE, Asano A, McElwee JL, Wolff CA, Nelson JL, Klaus AV, Hunnicutt GR, and Travis AJ (2007). GM1 dynamics as a marker for membrane changes associated with the process of capacitation in murine and bovine spermatozoa. J. Androl. 28, 588–599. [PubMed: 17377143]

Singh AK, McGoldrick LL, Twomey EC, and Sobolevsky AI (2018). Mechanism of calmodulin inactivation of the calcium-selective TRP channel TRPV6. Sci. Adv 4, eaau6088. [PubMed: 30116787]

Smith JF, Syritsyna O, Fellous M, Serres C, Mannowetz N, Kirichok Y, and Lishko PV (2013). Disruption of the principal, progesterone-activated sperm Ca2+ channel in a CatSper2-deficient infertile patient. Proc. Natl. Acad. Sci. USA 110, 6823–6828. [PubMed: 23530196]

Strünker T, Goodwin N, Brenker C, Kashikar ND, Weyand I, Seifert R, and Kaupp UB (2011). The CatSper channel mediates progesterone-induced Ca2+ influx in human sperm. Nature 471, 382–386. [PubMed: 21412338]

Suarez SS, Varosi SM, and Dai X (1993). Intracellular calcium increases with hyperactivation in intact, moving hamster sperm and oscillates with the flagellar beat cycle. Proc. Natl. Acad. Sci. USA 90, 4660–4664. [PubMed: 8506314]

Tamura K, Stecher G, Peterson D, Filipski A, and Kumar S (2013). MEGA6: Molecular Evolutionary Genetics Analysis version 6.0. Mol. Biol. Evol. 30, 2725–2729. [PubMed: 24132122]

Van Petegem F, Chatelain FC, and Minor DL Jr. (2005). Insights into voltage-gated calcium channel regulation from the structure of the CaV1.2 IQ domain-Ca2+/calmodulin complex. Nat. Struct. Mol. Biol. 12, 1108–1115. [PubMed: 16299511]

Villén J, and Gygi SP (2008). The SCX/IMAC enrichment approach for global phosphorylation analysis by mass spectrometry. Nat. Protoc. 3, 1630–1638. [PubMed: 18833199]

Visconti PE, Bailey JL, Moore GD, Pan D, Olds-Clarke P, and Kopf GS (1995). Capacitation of mouse spermatozoa. I. Correlation between the capacitation state and protein tyrosine phosphorylation. Development 121, 1129–1137. [PubMed: 7743926]

Wang H, Liu J, Cho KH, and Ren D (2009). A novel, single, transmembrane protein CATSPERG is associated with CATSPER1 channel protein. Biol. Reprod. 81, 539–544. [PubMed: 19516020]

Wood CD, Nishigaki T, Furuta T, Baba SA, and Darszon A (2005). Real-time analysis of the role of Ca(2+) in flagellar movement and motility in single sea urchin sperm. J. Cell Biol. 169, 725–731. [PubMed: 15928204]

Yanagimachi R (1970). The movement of golden hamster spermatozoa before and after capacitation. J. Reprod. Fertil. 23, 193–196. [PubMed: 5472441]

Yanagimachi R (2017). The sperm cell: production, maturation, fertilization, regeneration (Cambridge University Press).

Yu FH, and Catterall WA (2004). The VGL-chanome: a protein superfamily specialized for electrical signaling and ionic homeostasis. Sci. STKE 2004, re15. [PubMed: 15467096]

Yue F, Cheng Y, Breschi A, Vierstra J, Wu W, Ryba T, Sandstrom R, Ma Z, Davis C, Pope BD, et al. ; Mouse ENCODE Consortium (2014). A comparative encyclopedia of DNA elements in the mouse genome. Nature 515, 355–364. [PubMed: 25409824]

Highlights

- *Efcab9* encodes an evolutionarily conserved, sperm-specific EF-hand domain protein
- *Efcab9*-deficient mice have sperm motility defects and compromised male fertility
- EFCAB9 senses both pH and Ca^{2+} helping regulate flagellar CatSper channel activity

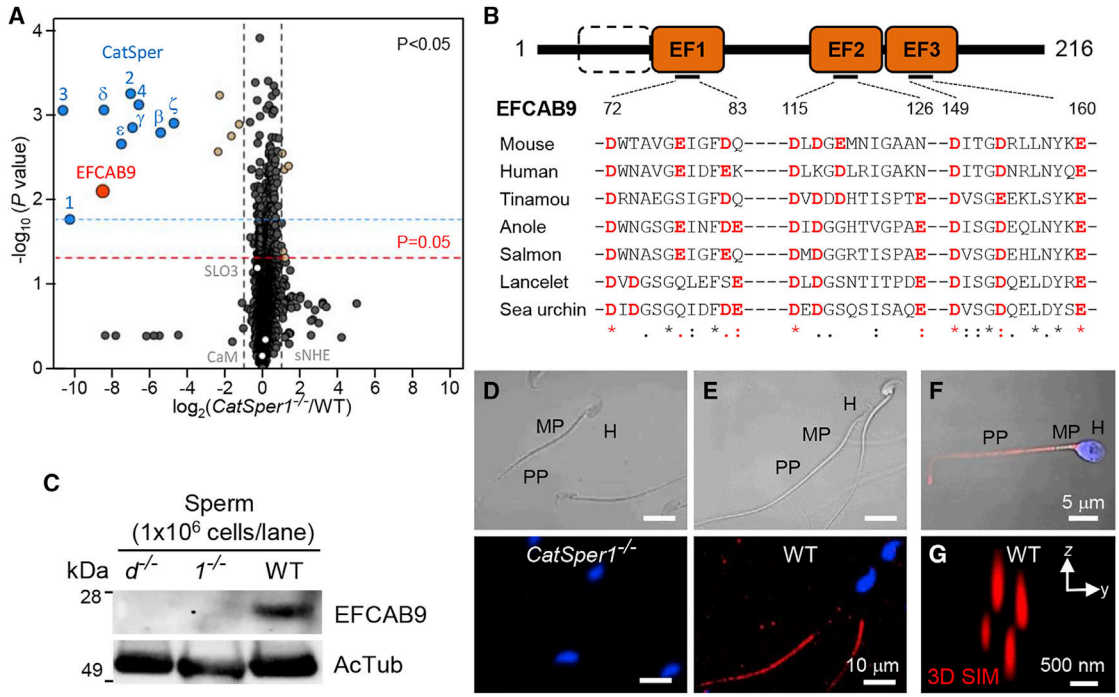

Figure 1. EFCAB9 Is an Intracellular Protein Associated with CatSper Channel Complex

(A) Quantitative analysis of whole sperm proteome from WT compared with *CatSper1*$^{-/-}$ mice. In volcano plot, each protein is represented as a dot and is mapped according to its average fold change in *CatSper1*$^{-/-}$ over WT spermatozoa on the x axis and t test p value on the y axis. EFCAB9 (orange dot) protein expression is one of the most reduced in *CatSper1*$^{-/-}$ spermatozoa, clustered together with other CatSper subunits (blue dots). The other nine proteins that are significantly differentially expressed are colored in tan.

(B) The predicted domain structure of mouse EFCAB9 protein. Mouse EFCAB9 contains 216 amino acids with three predicted EF-hand domains (filled boxes). Empty box indicates the non-EF hand counterpart region aligned to the first EF-hand domain of CaM. Conserved acidic amino acids in the loop regions of EF-hand domains are highlighted in red.

(C) EFCAB9 protein expression in WT sperm compared with *CatSper1*$^{-/-}$ and *CatSperd*$^{-/-}$ sperm by immunoblot of total sperm extract.

(D and E) Immunofluorescence confocal images of EFCAB9 protein in *CatSper1*$^{-/-}$ (D) and WT (E) sperm.

(F) Confocal immunofluorescent detection of EFCAB9 protein in human sperm. EFCAB9 (red) and Hoechst-stained DNA (blue) (D–F). The corresponding DIC images are shown for (D) and (E).

(G) A cross-section 3D SIM image of EFCAB9 in WT mouse sperm.

See also Figures S1 and S2 and Table S1.

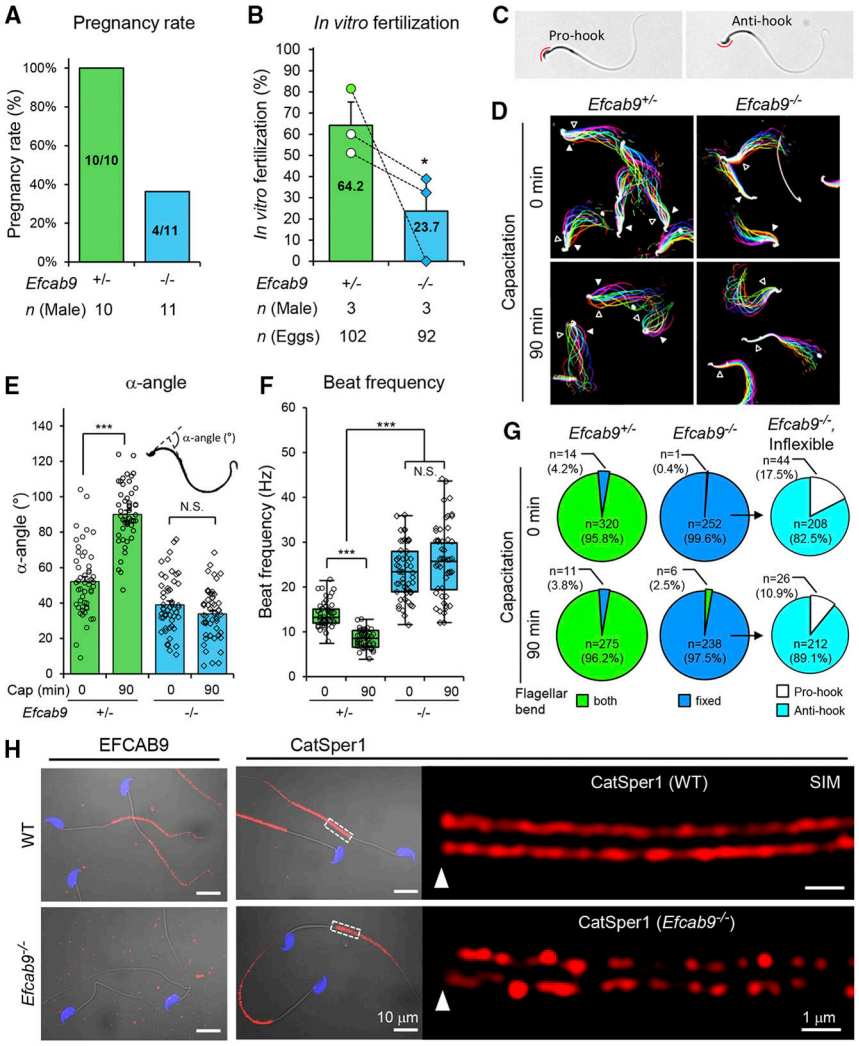

Figure 2. Genetic Disruption of *Efcab9* Compromises Male Fertility, Sperm Motility, and CatSper Domain

(A) Pregnancy rate of *Efcab9*$^{-/-}$ compared with *Efcab9*$^{+/-}$ males over 2 months when housed together with WT females.

(B) *In vitro* fertilization rate of *Efcab9*$^{+/-}$ (circles, 64.2% ± 11.0%) and *Efcab9*$^{-/-}$ (diamonds, 23.8% ± 14.7%) sperm with cumulus oocyte complex. Each dotted line indicates the results from each paired replication (n = 3). *p < 0.05.

(C) Flagellar bending of mouse sperm. Red lines indicate the curvature of the sperm head (hook). Pro-hook (left) and anti-hook (right) bends refer to the primary flagellar bend in the same or the opposite direction to the hook of the head, respectively. </p/> (D) Flagellar waveform of *Efcab9*$^{+/-}$ (left) and *Efcab9*$^{-/-}$ (right) sperm cells. Movies recorded at 200 fps from the head-tethered cells to glass coverslips before (top, 0 min) and after (bottom, 90 min) incubating under capacitation conditions. Overlays of flagellar traces from two beat cycles are time-coded in color. Pro-hook and anti-hook directions are marked with filled and empty arrows, respectively.

(E) The maximal bending angle of the midpiece (α-angle) in primary anti-hook curvature was measured from *Efcab9*$^{+/-}$ (0 min, 52.1° ± 2.7°; 90 min, 90.1° ± 2.3°) and *Efcab9*$^{-/-}$ (0

min, 40.0° ± 2.2°; 90 min, 33.8° ± 2.1°) sperm, and tail parallel to head is considered to 0°. Data are represented as mean ± SEM. n = 50 for each group. ***p < 0.001.

(F) Beat frequency before (0 min, *Efcab9*$^{+/-}$, 13.9 ± 0.4 Hz; *EFCAB9*$^{-/-}$, 23.5 ± 0.9 Hz) and after (90 min, *Efcab9*$^{+/-}$, 8.19 ± 0.27 Hz; *Efcab9*$^{-/-}$, 26.2 ± 1.2 Hz) incubating under capacitation conditions is shown in boxplot, indicating quartile distribution of individual data points. Median ± SEM, n = 50 each group (*Efcab9*$^{+/-}$, circles; *Efcab9*$^{-/-}$, diamonds). ***p < 0.001.

(G) Flagellar bending patterns of sperm from *Efcab9*$^{+/-}$ (left) and *Efcab9*$^{-/-}$ (middle and right) mice. Flagellar waveform were examined and classified into those bent in both directions (green) or in a fixed direction (blue). Sperm cells that beat in one direction are further divided into pro-hook (white) or anti-hook (cyan). Sperm numbers in the pie charts are from three independent experiments.

(H) *Efcab9*$^{-/-}$ spermatozoa have normal sperm morphology but display discontinuous CatSper domains. Overlay of confocal images and the corresponding DIC images of immunostained WT (top) and *Efcab9*$^{-/-}$ (bottom) sperm cells by α-EFCAB9 (left) and α-CatSper1 (right). SIM images at the right side of the CatSper1 confocal images are from the inset. Arrowhead indicates annulus, the junction between the midpiece and principal piece of the sperm tail.

See also Figures S3 and S4 and Video S1.

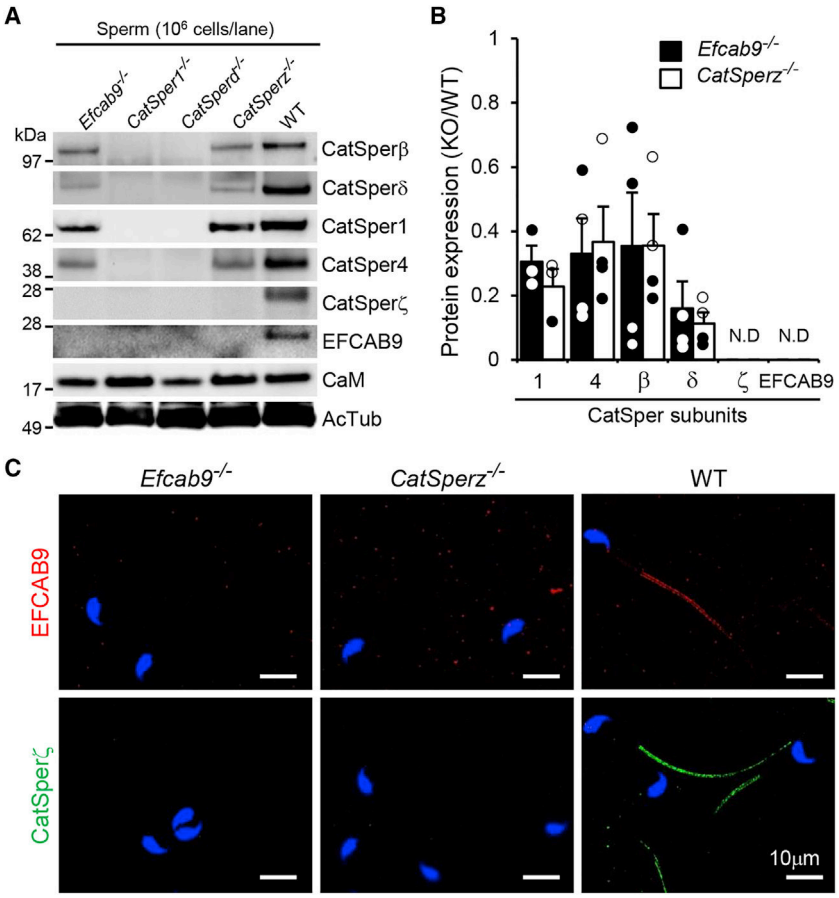

Figure 3. EFCAB9 and CatSperζ Form a Binary Complex in Spermatozoa

(A and B) EFCAB9 and CatSperζ proteins express interdependently in spermatozoa. (A) The absence of either EFCAB9 or CatSperζ is dispensable for the protein expression of all the TM CatSper subunits but eliminates the expression of each other. (B) Protein expression levels of CatSper subunits in *Efcab9*$^{-/-}$ and CatSperz$^{-/-}$ sperm compared with those of WT sperm. The relative levels of CatSper subunits detected in *Efcab9*$^{-/-}$ versus CatSperz$^{-/-}$ sperm are all comparable; CatSper1 (0.31 ± 0.05 versus 0.23 ± 0.06), CatSper4 (0.33 ± 0.11 versus 0.37 ± 0.11), CatSperβ (0.35 ± 0.16 versus 0.36 ± 0.10), and CatSperδ (0.16 ± 0.08 versus 0.11 ± 0.03). Each circle indicates fold changes of the protein expression in *Efcab9*$^{-/-}$ and *CatSperz*$^{-/-}$ spermatozoa quantified by measuring density of the bands from independent western blots (n = 3–4 from 4 males). Data are represented as mean ± SEM. (C) Confocal images of immunostained EFCAB9 (red) and CatSperζ (green) in *Efcab9*$^{-/-}$, *CatSperz*$^{-/-}$, and WT sperm. Hoechst dye stains sperm head (blue).

See also Figure S4.

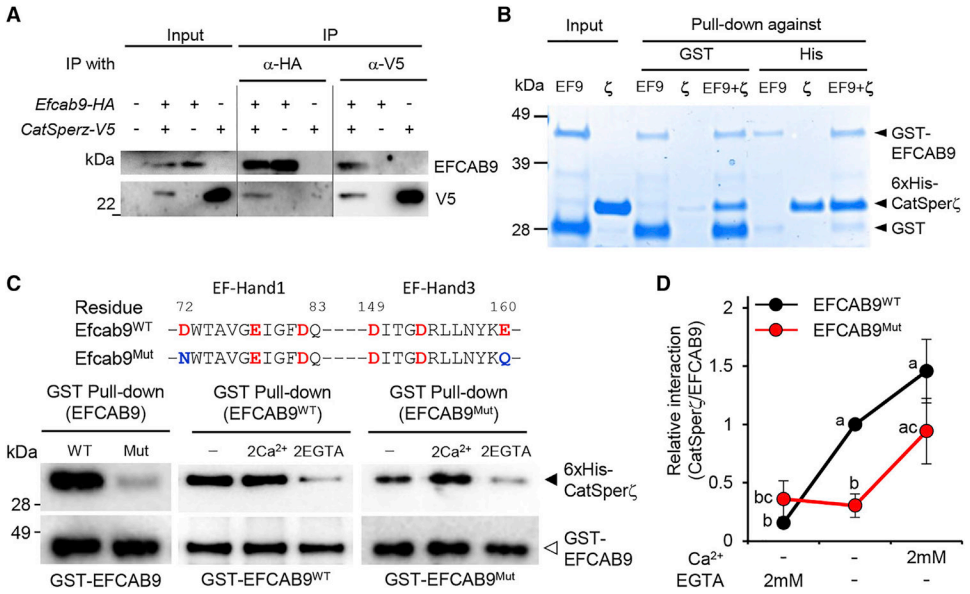

Figure 4. EFCAB9 Directly Binds to CatSperζ, and the Interaction Is Ca^{2+} Sensitive

(A) CoIP of EFCAB9 with CATSEPRζ. HA-tagged EFCAB9 and/or V5-tagged CatSperζ expressed in HEK293T cells were immunoprecipitated with anti-HA or anti-V5 and the immunocomplexes were blotted with anti-EFCAB9 or V5 antibodies.

(B) Pull-down analysis of purified recombinant EFCAB9 and CatSperζ proteins. GST or His pull-down analysis was performed between GST-EFCAB9 and 6xHis-CatSperζ fused to Gb1. Proteins are visualized by Coomassie blue staining.

(C) Ca^{2+}-dependent interaction between EFCAB9 and CatSperζ through the EF hands. The mutant is indicated as $EFCAB9^{Mut}$ (D72N/E160Q). The effect of mutations on the interaction with 6xHis-CatSperζ (left) was analyzed by GST pull-down assay in the binding buffer containing ~10 μM free Ca^{2+} as a trace ion (nominal free Ca^{2+}) at pH 7.5. Ca^{2+}-dependent interaction was further tested by GST pull-down between GST-EFCAB9 and 6xHis-CatSperζ in medium with nominal free Ca^{2+} (−), 2 mM $CaCl_2$ ($2Ca^{2+}$), or nominally calcium-free plus 2 mM EGTA (2EGTA) at pH 7.5 ($EFCAB9^{WT}$, middle; $EFCAB9^{Mut}$, right). GST-pulled EFCAB9 proteins serve as loading controls (empty arrow). Interacting target 6xHis-CatSperζ proteins are marked by a filled arrow.

(D) Relative amount of 6xHis-CatSperζ directly bound to GST pull-down EFCAB9. Protein levels in each pull-down condition in (C) are quantified by density of the bands from western blots. Relative amount of 6xHis-CatSperζ bound to $GST\text{-}EFCAB9^{WT}$ at nominally free Ca^{2+} condition, pH 7.5 is set to 1. Means with different letters are significantly different in pairwise comparisons between different Ca^{2+} concentrations or recombinant EFCAB9 proteins ($p < 0.05$). Data are represented as mean ± SEM, n = 5. All the recombinant proteins in (B)–(D) were purified from *E. coli*.

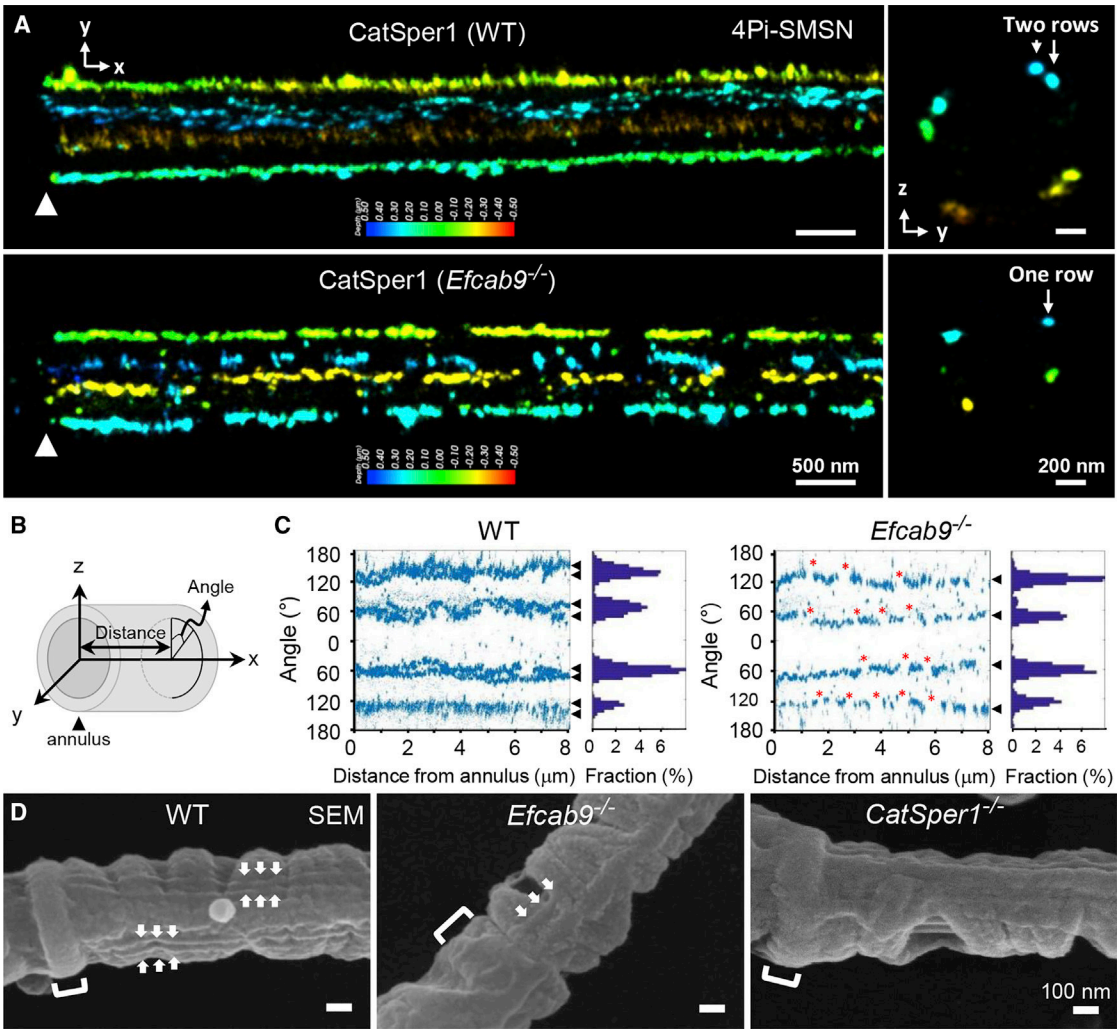

Figure 5. Loss of EFCAB9 Alters the Two-Row Structures of CatSper Domains and Sperm Surface Nanoarchitecture

(A) 3D 4Pi-SMSN images of CatSper1 in WT (top) and *Efcab9*$^{-/-}$ (bottom) flagella. x-y projection colors encode the relative distance from the focal plane along the z axis. Scale bar, 500 nm. Arrowheads in each panel indicate annulus. y-z cross sections (100 nm thick) at ~3 μm from the annulus are shown on the right. Two-row structures versus one-row structures within linear quadrants are marked with arrows. Scale bar, 200 nm.

(B) An illustrative cartoon of the angular plot to display surface molecular distributions in 2D. Molecules in the flagellar membrane were represented by angular distributions within a hollow cylinder with an inner radius of 300 nm, an outer radius of 500 nm, and the central axis placed at the flagellar center by converting molecular positions in the Cartesian (xyz) coordinates to the cylindrical coordinates.

(C) Angular distributions (left) and profile (right) of the surface-localized molecules of 4Pi-SMSN images of CatSper1 in WT (upper) and *Efcab9*$^{-/-}$ (lower) shown in (A). Arrowheads next to angular distributions indicate the rows within each CatSper quadrant. Red asterisks in angular distributions of *Efcab9*$^{-/-}$ sperm (right) indicate the gaps in each linear CatSper domain.

(D) SEM images of flagella from WT (left), *Efcab9*$^{-/-}$ (middle), and *CatSper1*$^{-/-}$ (right) mice. Two-row structure organization on the membrane surface are observed in both sides of longitudinal column in WT sperm but only one fragmented line in *Efcab9*$^{-/-}$ spermatozoa. No linear presentation is observed in *CatSper1*$^{-/-}$ sperm cells. Scale bar, 100 nm.
See also Videos S2 and S3.

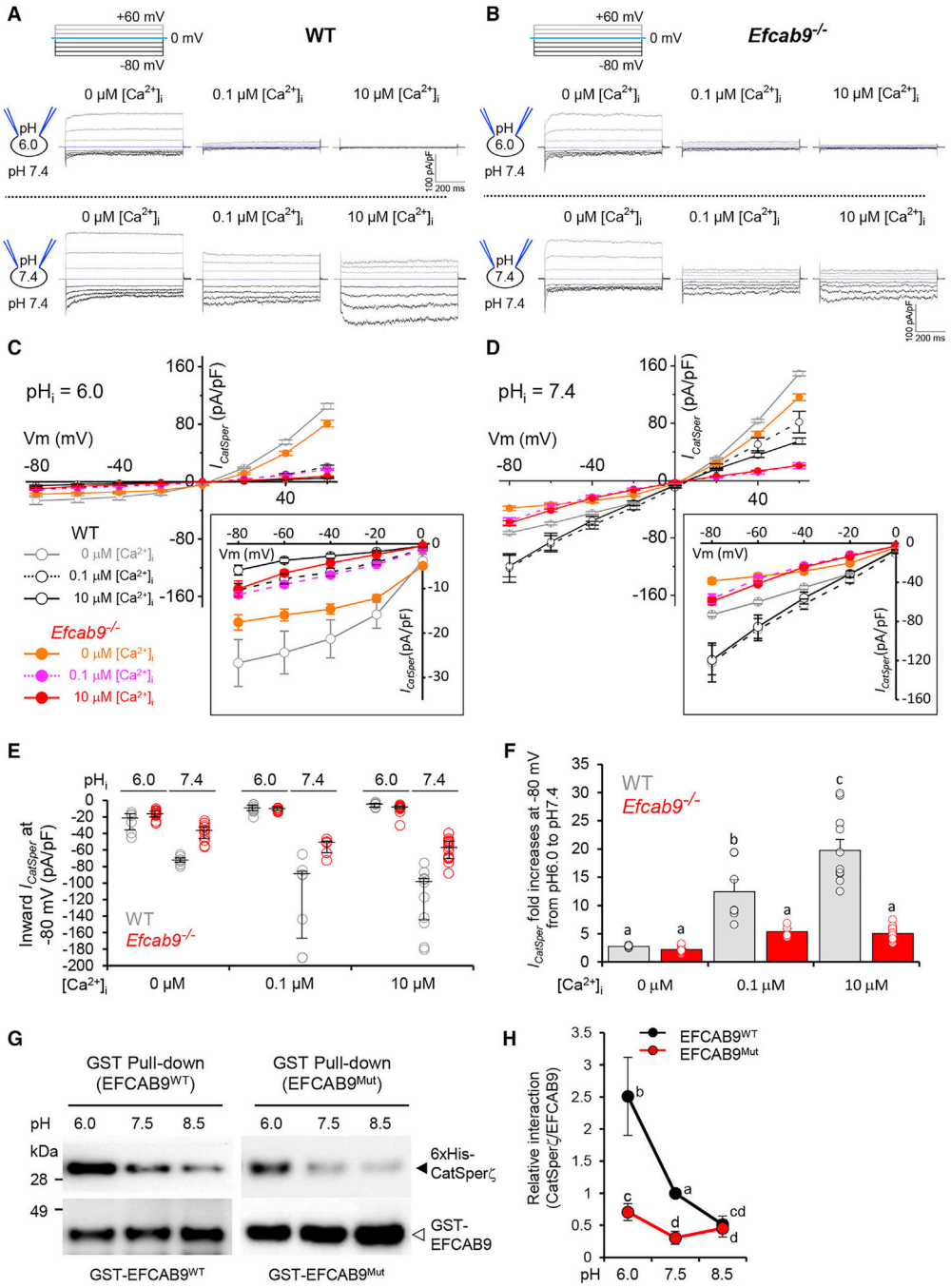

Figure 6. EFCAB9 Confers Maximal CatSper Channel Activity in a pH- and Ca^{2+}-Dependent Manner

(A and B) Representative $I_{CatSper}$ traces from WT (A) and *Efcab9*$^{-/-}$ (B) sperm recorded with 0 μM (left), 0.1 μM (middle), or 10 μM (right) free intracellular Ca^{2+} at intracellular pH = 6.0 (top) or intracellular pH = 7.4 (bottom). Currents were elicited by a step protocol from −80 mV to +60 mV in 20 mV increments and a holding potential of 0 mV. The cartoons indicate the intracellular and bath pH used for each panel.

(C and D) I-V relationship of $I_{CatSper}$ traces deducted at steady-state levels from recordings of WT (empty circles) and *Efcab9*$^{-/-}$ (filled circles) sperm with 0 μM, 0.1 μM, or 10 μM

free intracellular Ca^{2+} at pH_i = 6.0 (C) and pH_i = 7.4 (D). The inset in each panel is a magnified view showing the inward current.

(E) Inward $I_{CatSper}$ from individual WT (gray) and *Efcab9*$^{-/-}$ (red) sperm collected at −80 mV at different intracellular Ca^{2+} concentrations. Horizontal lines in columns show quartile distribution of $I_{CatSper}$.

(F) Bars represent fold increase of the inward $I_{CatSper}$ at −80 mV when switching from intracellular pH 6.0 to pH 7.4 in WT (gray) and *Efcab9*$^{-/-}$ (red) sperm. Fold-increases are quantified by normalization with each averaged $I_{CatSper}$ at pH 6.0 at respective conditions. Means with different letters are significantly different in pairwise comparisons between genotypes or Ca^{2+} concentrations. $p < 0.05$.

(G) EFCAB9-CatSperζ complex dissociates when pH increases from 6.0 to 8.5. GST pull-down analysis was performed between GST-EFCAB9 (WT, left; Mut, right) and 6xHis-CatSperζ under the increasing pH conditions at pH 6.0, 7.5, and 8.5. Binding buffer contains ~10 μM free Ca^{2+} as a trace ion (without adding any additional calcium ions). CatSperζ (filled arrow) interacting with EFCAB9 (empty arrow, loading control) are detected by western blots.

(H) Quantitation of relative CatSperζ bound to EFCAB9. 6xHis-CatSperζ bound to GST-EFCAB9^{WT} is reduced by raising pH while the interaction with GST-EFCAB9^{Mut} is changed little to none. EFCAB9^{Mut} shows significantly reduced interaction with CatSperζ compared with EFCAB9^{WT} at pH 6.0 and pH 7.5, respectively. Means with different letters are significantly different in pairwise comparisons between different pH conditions or recombinant EFCAB9 proteins. All the recombinant proteins were purified from *E. coli* as in Figure 4. Data are represented as mean ± SEM (C–F and H). n = 5.

See also Figure S5.

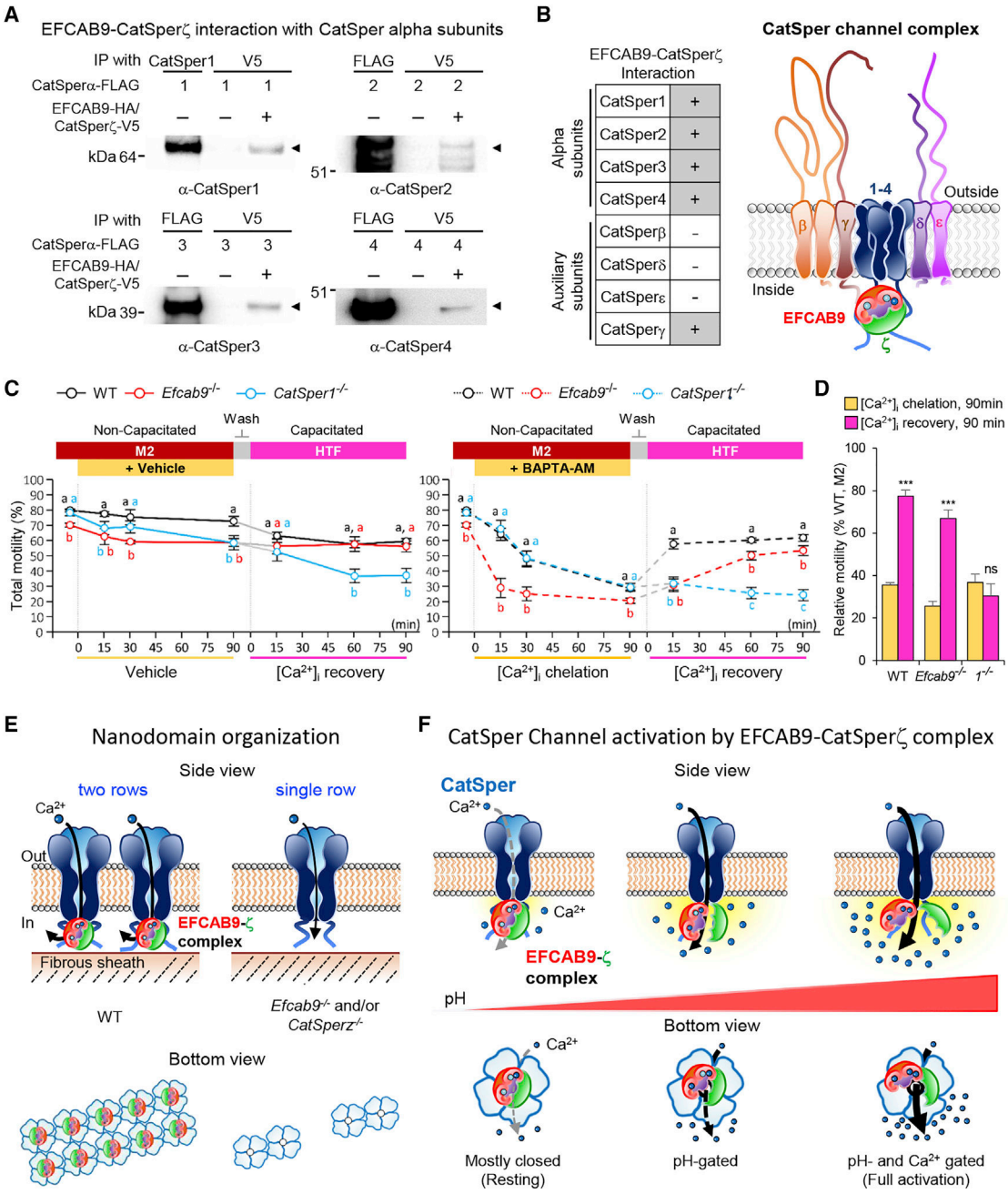

Figure 7. EFCAB9-CatSperζ Interacts with the Channel Pore and Senses Intracellular Ca^{2+} Changes

(A) Molecular interaction of EFCAB9-CatSperζ with other CatSper subunits. CoIP assays were performed from 293T cells transfected with plasmids encoding CatSperζ-V5-(P2A)-EFCAB9-HA and one of each CatSper alpha subunit (1, 2, 3, or 4). After immunoprecipitation with anti-V5 resin, precipitates were analyzed by immunoblotting with antibodies against each CatSper protein.

(B) Summary of interaction between EFCAB9-CatSperζ complex and TM CatSper subunits. Based on the coIP experiments in (A) and Figure S7, positive or negative interactions are

marked with gray or white cells, respectively (left). The cartoon illustrates the interaction and predicted topology of the 10 subunits of mammalian CatSper channel complex (right). (C and D) Effect of intracellular Ca^{2+} handling on sperm motility from WT, *Efcab9*$^{-/-}$, and *CatSper1*$^{-/-}$ males. Uncapacitated epididymal sperm (M2) were loaded with vehicle or 5 μM BAPTA-AM (membrane-permeable Ca^{2+} chelator) that buffers $[Ca^{2+}]_i$ at low nM levels. The pre-incubated sperm were then allowed to recover $[Ca^{2+}]_i$ by incubating during capacitation (HTF). Sperm motility was analyzed by CASA for each time point from WT (black; n = 4), *Efcab9*$^{-/-}$ (red; n = 3 with 2 *Mut* 5*del* and 1 *Mut* 28*del*), and *CatSper1*$^{-/-}$ (blue; n = 4) mice. (C) Total motility (%) of sperm treated with vehicle (left) or BAPTA-AM (right). Means with different letters indicate significant difference in pairwise comparison between genotypes at each point, but not between time points within a genotype. Data are represented as mean ± SEM. (D) Relative motility change by $[Ca^{2+}]_i$ chelation (orange) and recovery (magenta) at 90-min incubation time point. Motility after $[Ca^{2+}]_i$ chelation and recovery was normalized by the average motility of WT sperm before pre-incubating with BAPTA-AM (M2, 0 min). Statistical analysis was performed between chelating and recovering $[Ca^{2+}]_i$ at 90 min within each genotype. p* < 0.05, p** < 0.01, and p*** < 0.001. Data are represented as mean ± SEM.

(E) CatSper nanodomain organization in WT and EFCAB9- and/or CatSperζ-deficient sperm.

(F) Proposed model for CatSper channel activation by EFCAB9-CatSperζ complex. Intracellular pH elevation during capacitation partially dissociates EFCAB9 from CatSperζ, which releases gate inhibition and opens the pore, enabling EFCAB9 to bind entering Ca^{2+} and undergo a conformational change to maintain the prolonged open state of the channel. See also Figures S6 and S7 and Videos S4, S5, and S6.

KEY RESOURCES TABLE

REAGENT or RESOURCE	SOURCE	IDENTIFIER
Antibodies		
Rabbit polyclonal anti-mCatSper1	Laboratory of David E. Clapham; Ren et al., 2001	Cat#CatSper1; RRID:AB_2314097
Rabbit polyclonal anti-mCatSper2	Laboratory of David L. Garbers; Quill et al., 2001	N/A
Rabbit polyclonal anti-mCatSper3	Laboratory of David E. Clapham; Qi et al., 2007	N/A
Rabbit polyclonal anti-mCatSper4	Laboratory of David E. Clapham; Qi et al., 2007	N/A
Rabbit polyclonal anti-mCatSperβ	Laboratory of David E. Clapham; Chung et al., 2011	N/A
Rabbit polyclonal anti-mCatSperδ	Laboratory of David E. Clapham; Chung et al., 2011	N/A
Rabbit polyclonal anti-mCatSperζ	Laboratory of Jean-Ju Chung; Chung et al., 2017	N/A
Rabbit polyclonal anti-hCatSperζ	Laboratory of Jean-Ju Chung; Chung et al., 2017	N/A
Rabbit polyclonal anti-mEFCAB9	This study	N/A
Rabbit polyclonal anti-GFP (FL)	SantaCruz	Cat# sc-8334; RRID:AB_641123
Mouse monoclonal anti-PMCA4 (clone JA9)	Novus Biologicals	Cat# NB300-569; RRID: AB_2061726
Mouse monoclonal anti-Flag (clone M2)	Sigma-Aldrich	Cat# F3165; RRID:AB_259529
Mouse monoclonal anti-acetylated tubulin	Sigma-Aldrich	Cat# 7451; RRID:AB_609894
Mouse monoclonal anti-Calmodulin	Upstate	Cat# 05-173; RRID:AB_309644
Mouse monoclonal anti-phosphotyrosine (clone 4G10)	EMD Millipore	Cat# 05-321; RRID:AB_309678
Mouse monoclonal anti-HA (clone 2–2.2.14)	Pierce	Cat# 26183; RRID:AB_2533056
Mouse monoclonal anti-MYC (clone 9E10)	SantaCruz	Cat# sc-40; RRID:AB_627268
Mouse monoclonal anti-HA (clone 6E2), HRP-conjugated	CST	Cat# 2999S; RRID:AB_1264166
Mouse monoclonal anti-MYC (clone 9B11), HRP-conjugated	CST	Cat# 2040S; RRID:AB_10707162
Mouse monoclonal anti-V5 (clone E10/V4RR), HRP-conjugated	Invitrogen	Cat# MA5-15253-HRP; RRID:AB_2537645
Goat anti-mouse IgG-HRP	Jackson ImmunoResearch	Cat# 115-035-003; RRID:AB_10015289
Goat anti-rabbit IgG-HRP	Jackson ImmunoResearch	Cat# 111-035-144; RRID:AB_2307391
Rat anti-mouse IgG Trueblot (clone eB144)	Rockland	Cat# 18-8817-31; RRID:AB_2610850
Anti-V5 Agarose Affinity Gel (clone V5-10)	Sigma Aldrich	Cat# A7345
Anti-HA Magnetic Beads (clone 2–2.2.14)	Pierce	Cat# 88836
Bacterial and Virus Strains		
NEB 10-beta Electrocompetent *E. coli* (High Efficiency)	NEB	Cat# C3019H
BL21-CodonPlus (DE3)-RIL competent cells	Agilent Technology	Cat# 230245
Chemicals, Peptides, and Recombinant Proteins		
EmbryoMax M2 Medium (1X), Liquid, with phenol red	EMD Millipore	Cat# MR-015-D
EmbryoMax Human Tubal Fluid (HTF) (1X), liquid, for Mouse IVF	EMD Millipore	Cat# MR-070-D

REAGENT or RESOURCE	SOURCE	IDENTIFIER
Dulbecco's Modified Eagle Medium (DMEM)	GIBCO	Cat# 12100-046
HAM's F12	GIBCO	Cat# 21700-075
FBS	Thermofisher	Cat# 10437-028
MG-132 (CAS 133407-82-6)	Calbiochem	Cat# 474790
Isopropyl β-D-thiogalactopyranoside (IPTG)	AmericanBio	Cat# AB00841
BAPTA-AM (CAS 126150-97-8)	Calbiochem	Cat# 196419
Pluronic F-127	Invitrogen	Cat# P3000MP
Dimethyl Sulfoxide, DMSO	AmericanBio	Cat# AB03091
Critical Commercial Assays		
Multiple Tissue Panels, cDNA (Mouse MTCTM Panel I)	Clontech	Cat# 636745
Deposited Data		
Raw images of immunoblot	This study	https://doi.org/10.17632/mv52ykks6x.1
BLASTP, NCBI Database	National Center for Biotechnology Information	https://blast.ncbi.nlm.nih.gov/Blast.cgi
BLASTP, JGI Database	Joint Genome Institute	https://genome.jgi.doe.gov
Mouse ENCODE transcriptome data	Yue et al., 2014	BioProject: PRJNA66167
Experimental Models: Cell Lines		
Human Embryonic Kidney (HEK) 293T	ATTC	Cat# CRL-3216; RRID:CVCL_0063
Human Embryonic Kidney (HEK) human CatSper1-GFP stable expression cell	Laboratory of David E. Clapham	N/A
Experimental Models: Organisms/Strains		
Mouse: B6.129S4-Catsper1$^{tm1Clph/J}$	Laboratory of David E. Clapham; Ren et al., 2001	RRID:IMSR_JAX:018311
Mouse: B6.129S4-Catsperd$^{tm1.1Clph/J}$	Laboratory of David E. Clapham; Chung et al., 2011	RRID:IMSR_JAX:021451
Mouse: Catsperz^{tm1Clph} (from ES cell line 1700019N12Rik$^{tm1(KOMP)Mbp}$)	Laboratory of David E. Clapham; Chung et al., 2017	N/A
Mouse:Efcab9^{tm1CHNG}	This study	N/A
Mouse:C57BL/6NCrl	Charles River Laboratories	Crl:029
Mouse:B6D2F1/Crl	Charles River Laboratories	Crl:099
Recombinant DNA		
Mammalian expression vector for mouse EFCAB9-HA (phCMV3-mEfcab9)	This study	N/A
Mammalian expression vector for mouse CatSperz-V5 (pCAG-mCatSperz-V5)	Laboratory of David E. Clapham	N/A
Mammalian bi-cystronical expression vector for mouse CatSperz-V5 and mouse EFCAB9-HA (phCMV3-mCatSperz-V5-P2A-mEfcab9)	This study	N/A
Mammalian expression vector for mouse CatSper1-Flag (phCMV3-mCatSper1-Flag)	This study	N/A
Mammalian expression vector for mouse CatSper2-Flag (phCMV3-mCatSper2-Flag)	This study	N/A
Mammalian expression vector for mouse CatSper3-Flag (phCMV3-mCatSper3-Flag)	This study	N/A

REAGENT or RESOURCE	SOURCE	IDENTIFIER
Mammalian expression vector for mouse CatSper4-Flag (phCMV3-mCatSper4-Flag)	This study	N/A
Mammalian expression vector for mouse Flag-CatSperb (pTracer2-Flag-mCaSperb)	Laboratory of David E. Clapham	N/A
Mammalian expression vector for mouse CatSperd (pcDNA3-mCatSperd)	Laboratory of David E. Clapham; Chung et al., 2011	N/A
Mammalian expression vector for mouse CatSperd-V5 (pCAG-mCatSperd-V5)	Laboratory of David E. Clapham; Chung et al., 2011	N/A
Mammalian expression vector for human EFCAB9-HA (phCMV3-hEFCAB9-HA)	This study	N/A
Mammalian expression vector for human CatSperz-V5 (phCMV3-hCatSpere-V5)	This study	N/A
Mammalian expression vector for Flag-human CatSpere (phCMV3-Flag-hCatSpere)	This study	N/A
Mammalian expression vector for Flag-human CatSperg (phCMV3-Flag-hCatSperg)	This study	N/A
Mammalian bi-cystronical expression vector for human EFCAB9-HA amd human CatSperz-MYC (pcDNA3.1(-)-hEfcab9-HA-P2A-hCatSperz-MYC)	This study	N/A
Bactrerial expression vector for GST-mouse EFCAB9 (pGEX-6P2-mEfcab9)	This study	N/A
Bactrerial expression vector for GST-mouse EFCAB9 (pET43a-mEfcab9)	This study	N/A
Bactrerial expression vector for 6xHis-pET32a-gb1-mCatSperzEFCAB9 (pET32a-gb1-CatSperz)	This study	N/A
Bactrerial expression vector for GST-mouse EFCAB9^{2Mut} (D72N/E160Q), (pGEX-6P2-mEfcab9^{2Mut}	This study	N/A
Bactrerial expression vector for GST-mouse EFCAB9^{4Mut} (D72N/D82N and D149N/E160Q), (pGEX-6P2-mEfcab9^{4Mut})	This study	N/A
Bacterial expression vector for GST-mouse CatSper1 N terminus (1–150) (pGex-2T-mCatSper1-N150)	Laboratory of David E. Clapham	N/A
Bacterial expression vector for mouse 6xHis-CatSper1 C terminus (574–686)-Flag (pET32a-mCatSper1-C-Flag)	This study	N/A
Mouse Efcab9 ORF clone 6771929	Dharmacon	Cat# MMM1013-202843024
Human Efcab9 ORF clone OHu00121D	GenScript	Cat# OHu00121D
Human CatSpere ORF clone 5269307	Dharmacon	Cat# MHS6278-202808312
Human CatSpere ORF clone 4823002	Dharmacon	Cat# MHS1010-202742776
pGEX-6P2	GE Healthcare	Cat# 28954650
pET43.1a(+)	Novagen	Cat# 70939
pET32a(+)	Novagen	Cat# 69015
Software and Algorithms		
Fiji	Schindelin et al., 2012	http://fiji.sc
Zen 2012 SP2	Carl Zeiss	https://www.zeiss.com/microscopy/us/products/microscope-software/zen-lite.html
SCA evolution	Microptic	https://www.micropticsl.com
R	R Foundation	https://www.r-project.org/
MEGA6	Tamura et al., 2013	https://www.megasoftware.net/

REAGENT or RESOURCE	SOURCE	IDENTIFIER
Other		
Glutathione agarose	Pierce	Cat# 16100
HisPur Ni-NTA Resin	Pierce	Cat# 88221
Protein A/G PLUS-Agarose	SantaCruz	Cat# sc-2003
SureBeads Protein A Magnetic Beads	BioRad	Cat# 1614011
SureBeads Protein G Magnetic Beads	BioRad	Cat# 1614021
CellVision 4 Chamber 20 micron	CellVision	Cat# CV 1020-4CH